Preparation and Characterisation of Vertically Aligned Carbon Nanotubes

---

A thesis

submitted in partial fulfilment

of the requirements for the degree of

Masters of Science in Chemistry

at the

University of Canterbury

by

Rui Xu

University of Canterbury

2010

Acknowledgements

I would like to thank my supervisors Prof. Alison Downard and Dr. Vladimir Golovko for their help and guidance with this work. Much thanks also goes to Danny Leonard for his assistance. I would also like to thank my research group members Dr. Xiaoming Liu and David J. Garrett for their help.

Table of Contents

Chapter 4: Synthesis of CNTs using Thermal CVD

Abstract

This thesis presents the preparation of vertically aligned carbon nanotubes using porous anodic alumina templates via thermal chemical vapour deposition. The characteristics of prepared carbon nanotubes in terms of tube diameter, length, density, uniformity and alignment were investigated.

The formation of porous anodic alumina membranes was studied. In order to prepare well-ordered porous anodic alumina templates, three approaches towards anodization of aluminium were examined. Effects of Al surface morphology and anodization conditions on the formation of the porous anodic alumina membrane were investigated.

Co catalyst was electrochemically deposited at the bottom of the pores of porous anodic alumina templates by applying an alternating current. Prior to the AC electrodeposition, the barrier layer at the base of the pores was thinned in order to facilitate the deposition process. The thinning effect of three barrier layer thinning approaches was examined. The effect of electrodeposition duration on the pore filling was investigated.

Carbon nanotubes were grown using Co-loaded porous anodic alumina templates via thermal chemical vapour deposition of C_2H_4. Effects of the presence of the Co catalyst, the amount of Co deposited at the bottom of the pores and the presence of water vapour on the carbon nanotube growth were examined. The characteristics of the grown carbon nanotubes in terms of tube diameter, length, density, uniformity and

alignment were investigated. Moreover, a post-treatment after the carbon nanotube growth was proposed in order to obtain vertically aligned carbon nanotubes.

In addition, vertically aligned carbon nanotubes were grown on Si chips. Two methods were used to prepare a catalytic layer on the Si chips for carbon nanotube growth.

Chapter 1: Introduction

1.1 Carbon Nanotubes

The discovery of carbon nanotubes (CNTs) have opened a new era in nanotechnology and material science. There are two main types of carbon nanotubes that can have high structural perfection. In 1976, Morinobu Endo and co-workers[1] published the first high resolution transmission electron microscopy (HRTEM) image of a single-walled carbon nanotube (SWNT) as shown in Fig 1.1A. They reported that it was possible to obtain tubular graphite of nanometer scale by pyrolysis of benzene and hydrogen at about 1100 °C.

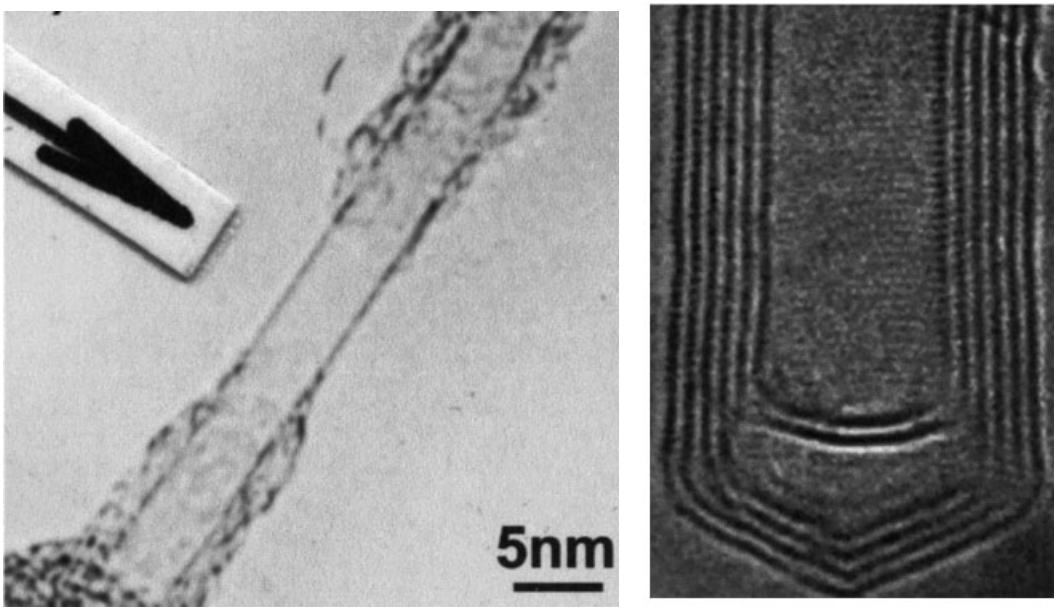

Fig 1.1 HRTEM image of (A) an individual graphene tube (adopted from reference 1), and (B) a multi-walled carbon nanotube (MWNT) (adopted from reference 2).

In 1991, Sumio Iijima[2] showed a HRTEM image of the structure of a multi-walled carbon nanotubes as shown in Fig 1.1B.

Carbon nanotubes may be viewed as a graphene sheet that is rolled up into a nanoscale tube i.e. SWNTs, or with additional graphene tubes around the core of a SWNT, i.e. MWNTs as shown in Fig 1.2 [3],[4],[5].

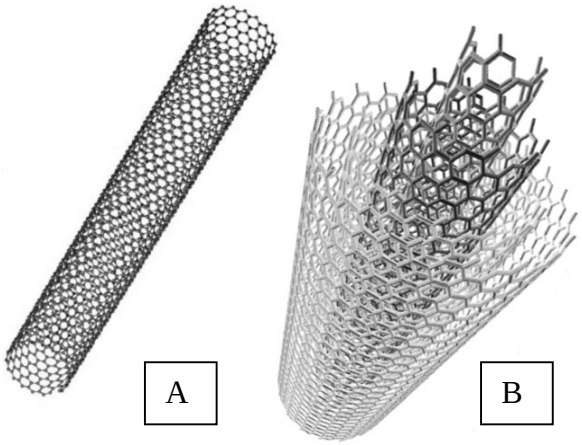

Fig 1.2 Schematic drawing of (A) a SWNT and (B) a MWNT.
(Adopted from reference 5)

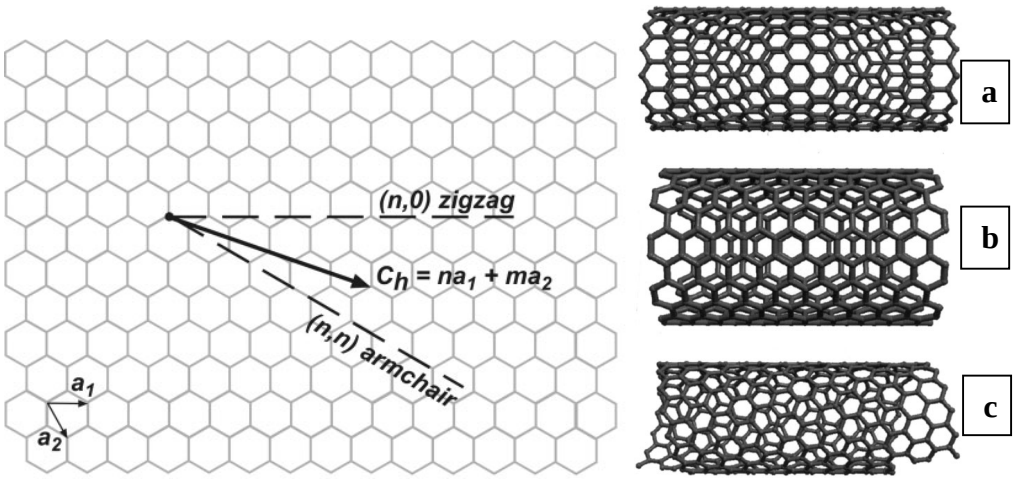

Fig 1.3 Models of nanotubes with different chirality showing the rolling of a graphene sheet along different chiral vectors. (Chiral vector of the hexagonal lattice: $\mathbf{C_h}=n\mathbf{a_1}+m\mathbf{a_2}$, where $\mathbf{a_1}$ and $\mathbf{a_2}$ are primitive vectors, n and m are integers.)
(a) zigzag arrangement; (b) armchair configuration; (c) chiral conformation
(Adopted from references 4 and 5)

A very important characteristic of carbon nanotubes is the tube chirality that describes how the graphene sheet is rolled up around the tube axis. The tube chirality can be defined in terms of a chiral vector $\mathbf{C_h}=n\mathbf{a_1}+m\mathbf{a_2}$, which can determine the tube diameter[5]. This vector determines the direction of rolling a graphene sheet, and there are 3 classes of configuration: zigzag (when m=0), armchair (when n=m) and chiral as shown in Fig 1.3. In the armchair configuration, two C-C bonds on opposite sides of each hexagon are perpendicular to the tube axis, whereas, in the zigzag configuration, these bonds are parallel to the tube axis. All other configurations, where the C-C bonds lie at an angle to the tube axis, are known as 'chiral' configurations (Fig 1.3).

Carbon nanotubes can exhibit semiconducting or metallic behaviour depending on their diameter and the tube chirality, even though there is no difference in the chemical bonding between the carbon atoms within the tubules[4],[5]. The unique electronic properties of carbon nanotubes are believed to be due to the quantum confinement of electrons normal to the nanotube axis (electrons can propagate only along the nanotube axis). In the radial direction, electrons are confined by the monolayer thickness of the graphene[4].

Carbon nanotubes usually have a diameter ranging from a few angstroms to tens of nanometers, and a length of up to several centimeters. Since the C-C bond in graphite is one of the strongest in nature, carbon nanotubes are very robust. Similar to the electronic properties, the tube stiffness may be dependent on chirality (e.g. zigzag tubes would be less stiff than armchair tubes)[6]. Ebbesen *et al.*[7] reported a very high average Young's modulus of 1-1.8 TPa for individual MWNTs. Falvo *et al.*[8]

reported that MWNTs could be bent repeatedly under large strain. This indicates that carbon nanotubes are also very flexible.

The thermal conductivity of carbon nanotubes, along the tube axis, may be one of the highest when compared to other materials. McEuen's group has determined the thermal conductivity of individual MWNTs, which is higher than that of graphite (3000 W/K) at room temperature[9]. Yi *et al.*[10] found that the thermal conductivity varies linearly with temperature from 4 to 300 K in MWNTs, and the specific heat of MWNTs produced by pyrolytic methods behaves linearly with temperature between 10 and 300 K. This result is in good agreement with the calculated specific heat of graphite, thus indicating a relatively weak interlayer coupling in MWNTs and graphite[10].

1.2 Applications of Carbon Nanotubes

Carbon nanotubes (CNTs) have generated a great interest for a broad range of applications[11],[12],[13], due to their unique mechanical, electronic and thermal properties[14],[15]. A few examples of their applications are described below.

- *Field Emission Sources*

Electrons can be easily emitted from carbon nanotube tips when a potential is applied between a carbon nanotube surface and an anode[16]. Therefore, carbon nanotubes

are advantageous in the fabrication of different types of efficient field emission sources[17], for example, flat panel displays, intense light sources or bright lamps, and X-ray sources. Some main advantages of using carbon nanotubes as electron emission devices are[4]:

- Stable field emission over prolonged time periods
- Low emission threshold potentials
- High current densities
- Absence of requirement for ultrahigh vacuum

- *Electrochemical Devices: lithium ion batteries and supercapacitors*

Carbon nanotubes are excellent material for electrochemical applications due to their large surface area[13]. Frackowiak and Beguin[18] demonstrated that carbon nanotubes could be used in lithium ion batteries and supercapacitors. Arrays of aligned MWNTs could be used in the anode fabrication for lithium ion batteries, and the intercalation capacity (490 mAh /g) is double that of standard carbon[19]. Polypyrrole/MWNT composites can reach specific capacitances of ~ 163 F/g. The MWNT supercapacitors can be used for applications that require high power capabilities and high storage capacities such as hybrid electric vehicles[13].

- *Gas Storage*

The inner hollow channel in carbon nanotubes could be used as a container to store various gases. Liu *et al.*[20] and Dillon *et al.*[21] have reported that hydrogen can be stored inside nanotubes. Ar could be introduced using high Ar pressures for 48 h at

650 °C. Terrones *et al.*[22] demonstrated that it is also possible to introduce N_2 inside MWNTs.

- *Scanning Probe Tips*

MWNTs have been successfully attached to scanning probe microscope silicon tips in order to enhance image resolution[23]. The superior mechanical strength of carbon nanotubes and the flexibility to bend and recoil makes carbon nanotubes an excellent material for the production of long-life microscope tips[24].

- *Molecular Sensors*

Wong *et al.*[25] demonstrated that it was possible to sense functional chemical groups attached at the nanotube ends using chemical force microscopy. Kong *et al.*[26] carried out toxic gas sensing experiments using SWNT circuits and pellets. Varghese *et al.*[27] demonstrated that MWNTs could also be used as efficient sensors for NH_3, H_2O, CO and CO_2.

1.3 Carbon Nanotube Fabrication

The synthesis methods of CNTs can be divided into three main classes: arc discharge, laser ablation and chemical vapour deposition (CVD). All these synthesis methods use metal catalysts such as Fe, Co, or Ni, for the nucleation and growth of CNTs. Depending on the synthesis procedures, the metals can be mixed with carbonaceous

solid electrodes (arc discharge) or with the target (laser ablation), or deposited (CVD) to form nanoclusters on the substrate surface[4],[5]. Different structures can be obtained depending on synthesis parameters.

- *Arc discharge*

Fabrication of CNTs using arc discharge involves passage of a direct current through two high purity graphite electrodes (separation about 1–2 mm) in a helium atmosphere. During arcing, a deposit forms on the cathode, while the anode is consumed. This deposit exhibits a cigar-like structure and it contains carbon nanotubes and nested polyhedral graphene particles[2]. Two main CNT growth mechanisms for the formation of individual MWNTs using arc discharge have been proposed. Iijima and co-workers[28],[29] first proposed that carbon atoms attach to the open edges of a growing carbon cylinder, which closes when conditions are not suitable for growth. Alternatively, Endo and Kroto[30] proposed that nanotubes are essentially elongated giant fullerenes, which grow by direct insertion of carbon speices from the vapour phase into the closed network.

The arc discharge techniques involves high purity graphite electrodes, metal powders as well as high purity He and Ar gases, hence the costs of making CNTs are high.

- *Laser ablation*

The use of high power lasers in conjunction with high temperature furnace offers an alternative production route to carbon nanotubes.

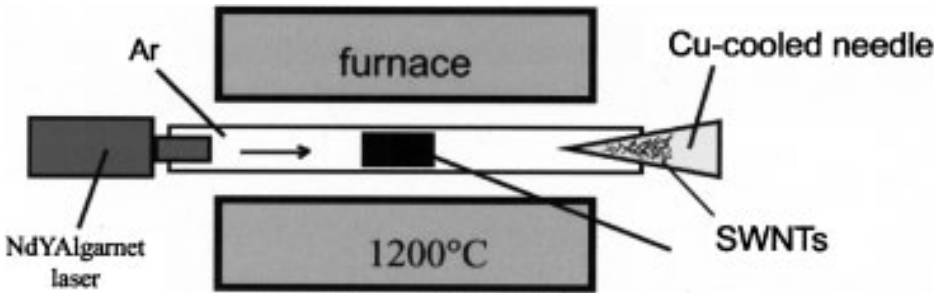

Fig 1.4 Experimental set-up for production of carbon nanotubes using laser ablation. (Adopted from reference 4)

In this method, a high purity graphite target is vaporized by a high power laser in a silica tube in Ar atmosphere, inside of a furnace at 1200 °C. Carbon nanotubes are collected from Cu-cooled water trap as shown in Fig 1.4 [31]. The CNT growth mechanism has been explained in terms of the attachment of incoming carbon species at the edges of adjacent growing graphene tubules, which finally results in a multilayered tube[31].

Similar to arc discharge method, laser ablation is not economically advantageous because the process involves high purity graphite rods, high power lasers and the yield of CNTs is low[4].

- *Chemical vapour deposition*

Chemical vapour deposition of carbon nanotubes is essentially a two-step process consisting of a catalyst preparation step followed by the actual synthesis of the nanotubes. The catalyst can be prepared by wet chemistry or by a sputtering process.

In the first case, a metal salt solution is applied to a substrate surface[32]. In the second case, a metal catalyst layer is deposited on a substrate by sputtering. The CVD system can be divided into two classes according to the actual synthesis process: plasma-enhanced CVD (PECVD) and thermal CVD.

In PECVD, plasma generated by hot filaments (HF) or electrical discharges at different frequencies (DC, RF, MW) is used to decompose and activate a carbon source gas. The reactive carbon species then diffuse towards the substrate loaded with metal catalyst to grow CNTs. Fig 1.5 shows a schematic view of a HFCVD reactor.

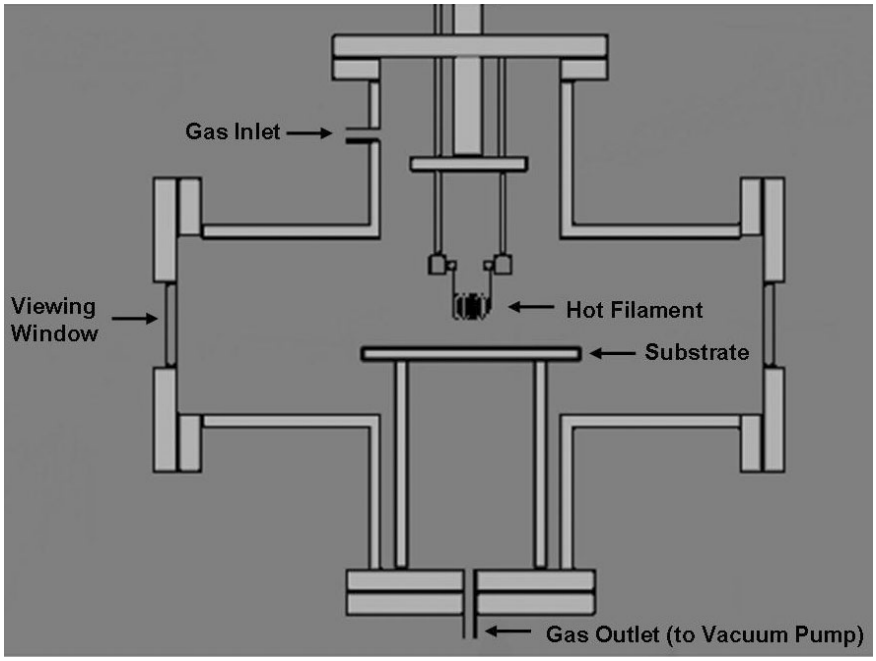

Fig 1.5 Schematic view of an HFCVD reactor for CNT synthesis
(Adopted from reference 5)

The thermal CVD makes use of a flow tube reactor inserted into a furnace for the thermal decomposition of a carbon source gas as shown in Fig 1.6.

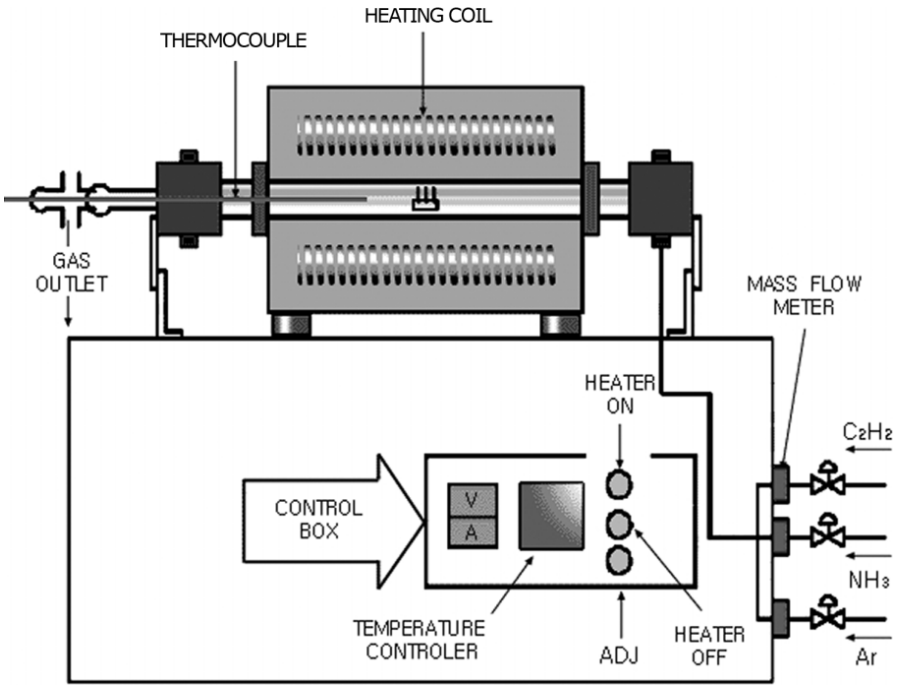

Fig 1.6 Scheme of apparatus for nanotube synthesis by thermal CVD (Adopted from reference 5)

In thermal CVD, a carbon source gas is passed over a surface coated with a metal catalyst at a high temperature, and deposition of the carbon on the surface is guided by the metal catalyst to form CNTs. Silicon is commonly used as a substrate for CNT growth, and recently, a range of conducting substrates have also been used such as titanium and planar graphitic carbon[33].

There are three proposed mechanisms to account for the CNT growth by CVD.

1. Tip carbon diffusion through catalytic particles

Baker *et al.*[34] postulated that decomposition of acetylene on the exposed surfaces of the metal catalyst resulted in the formation of bimolecular hydrogen and carbon species. The carbon then diffuses through the metal catalyst and precipitates at the other end of the filament in form of graphite and the metal particle always remains at the tip of tubule. This process is shown in the top of Fig 1.7.

2. Tip carbon diffusion on catalytic particles

Baird and Fryer[35] in 1974 and Oberlin *et al.*[1] in 1976 proposed that carbon filaments are formed by surface diffusion on the particle as shown in the middle of Fig 1.7

3. Bottom carbon diffusion through catalytic particles

This mechanism was based upon pyrolytic decomposition of acetylene passed over Fe–Pt substrates[36] In this case, growth occurs due to the rapid movement of carbon through the catalyst by a diffusion process, thus generating a filament as shown in the bottom of Fig 1.7.

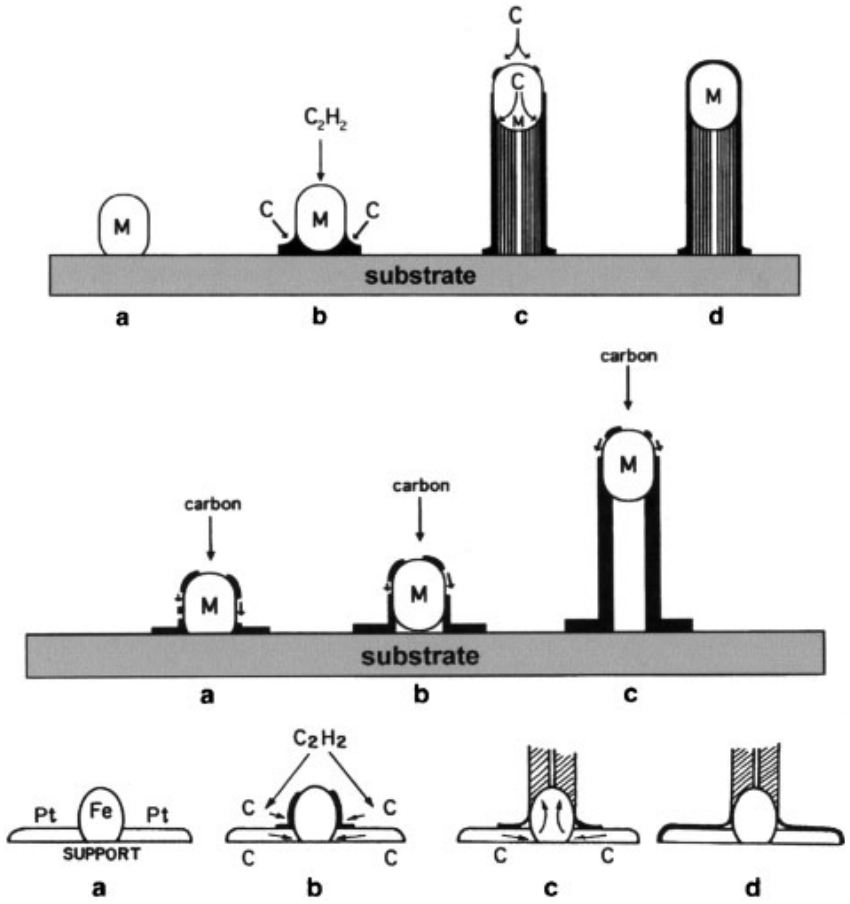

Fig 1.7 (Top) Tip growth through the metal catalyst. (Middle) Tip growth on the metal catalyst. (Bottom) Bottom growth through the metal catalyst. (Adopted from reference 4)

Among these synthesis methods, the CVD technique is commonly used because it allows production of dense carpets of CNTs that are vertically aligned due to steic crowding and van der Waals interactions between each neighbouring CNT[37]. By patterning the catalytic layer on the substrate surface, VACNT arrays with the same pattern as the catalytic layer can be fabricated[37]. Moreover, it is relatively cheap and can be easily scaled up, thus playing an important role in the mass production of carbon nanotubes with a low cost.

1.4 Templated Synthesis of Vertically Aligned Carbon Nanotubes

The synthesis of CNTs using a porous anodic alumina (PAA) template has drawn considerable attention due to its capability of producing highly ordered arrays of VACNTs with controllable dimensions[38]. This PAA template-based synthesis involves three steps as shown in Fig 1.8a. A PAA template is prepared by anodization of Al, and a metal catalyst is electrodeposited at the bottom of the pores the PAA template followed by CNT growth using a CVD system[39]. When CNTs nucleate and grow in the pores, the pores act as templates to confine the growth of the CNTs, making them well aligned along the pore walls as well as restricting the outer diameter to that of the pores[40]. Therefore, this approach allows fabrication of individual VACNTs as shown in Fig 1.8b.

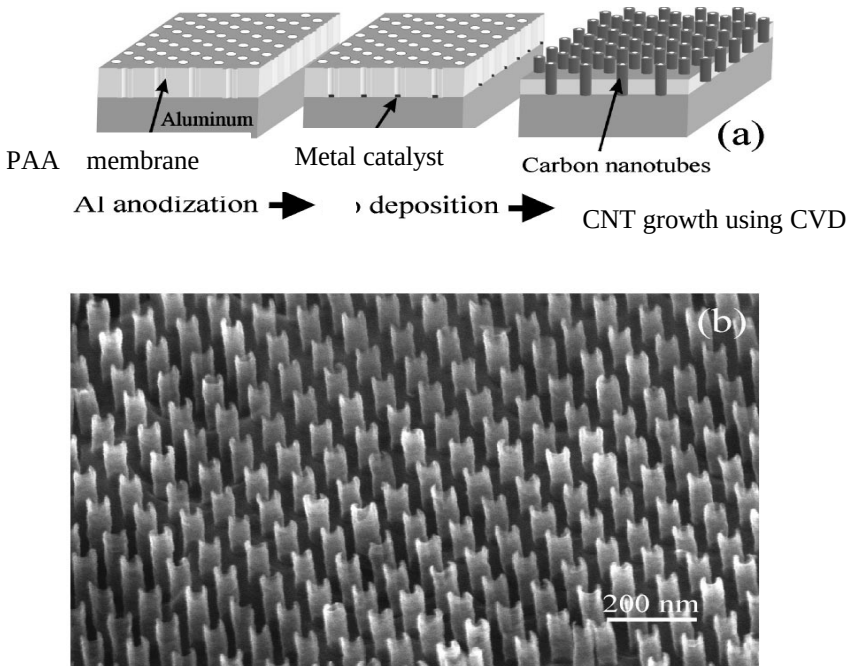

Fig 1.8 (a) A schematic diagram showing the template-synthesis process.
(b) SEM image of ordered VACNTs fabricated using this method
(Adopted from reference 39)

Jeong *et al.* [41] pointed out that synthesis of CNTs in a PAA template is a complex process which involves competitive carbon deposition on the metal catalyst particles and on the template itself. A schematic summary of CNT growth with a PAA template is shown in Fig 1.9.

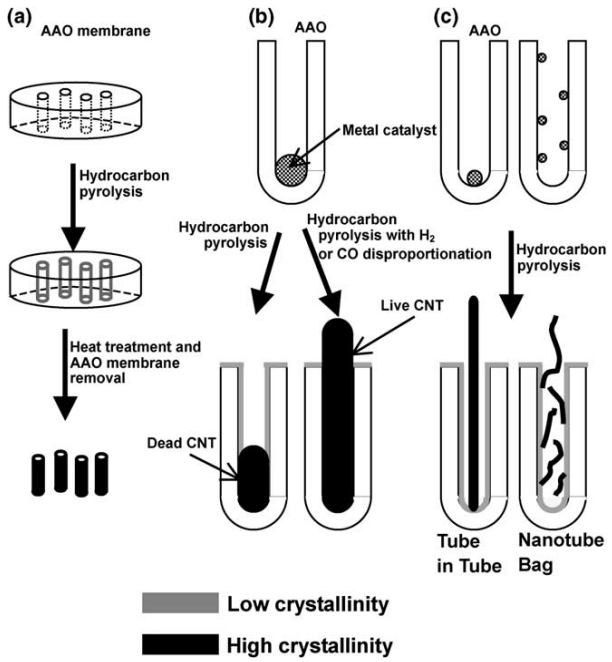

Fig 1.9 Schematic diagram of CNT growth with PAA template: (a) without metal catalyst, (b) with metal catalyst, left à absence of H_2, right à presence of H_2 and (c) with metal catalyst which has a smaller diameter than that of the PAA template. (Adapted from reference 41)

Fig 1.9 (a) is the case of hydrocarbon decomposition without metal catalyst. Carbon deposits inside of the pores. High temperature is crucial to achieve high crystallinity. In Fig 1.9 (b), the metal catalyst fills the entire space of the pore bottom so the diameter of a catalyst particle is the same as the pore. In this case, the growth of CNTs

depends strongly on the competition of two mechanisms: carbon deposition on the metal catalyst electrodeposited at the bottom of the pores and on the pore wall. Carbon deposits on the pore wall can easily block the growth of a CNT from the bottom, resulting in a dead CNT (left of Fig 1.9 b). Hydrogen can suppress the carbon deposition on the pore wall, resulting in overgrown CNTs (right of Fig 1.9 b). Fig1.9 (c) shows what happens when the size of a metal catalyst is much smaller than the diameter of a pore. In this case, carbon deposition on the pore wall does not block the growth of CNTs from the bottom. Therefore, the two mechanisms work independently and simultaneously. As a result, the crystalline CNTs grown from the bottom are encircled by the larger diameter amorphous carbon tubes templated by the pores, giving a tube-in-tube structure as shown in the left of Fig 1.9 (c) or a nanotube bag structure as shown in the right of Fig 1.9 (c).

1.5 Aims

In the case of CNTs grown in dense carpets, the vertical alignment of the CNTs results from steric crowding and van der Waals interactions between each neighbouring CNT. As a consequence, the minimum accessible diameter of VACNT bundles is confined to 2 μm as shown in Fig 1.10 reported by Liu *et al.*[37] a post-doctor who worked for Prof. Alison Downard.

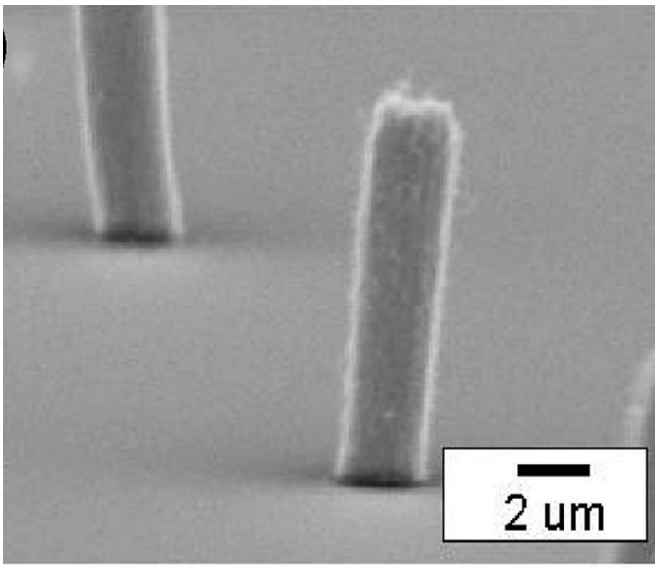

Fig 1.10 SEM image of patterned 2μm VACNT pillars grown using thermal CVD. (Adopted from reference 37)

In order to grow individual VACNTs, an alternative approach towards vertical alignment of CNTs is needed. In this research, porous anodic alumina templates embedded with metal catalyst were used to grow individual VACNTs via thermal CVD.

Specific goals were to:

1. Prepare well-ordered porous anodic alumina templates
2. Electrochemically deposit Co catalyst in the base of the pores of the PAA template
3. Grow VACNTs from the Co-loaded PAA template using thermal CVD

References

[1] A. Oberlin, M. Endo and T. Koyama, *Journal of Crystal Growth* **1976**, *32*, 335-349.
[2] S. Iijima, *Nature* **1991**, *354*, 56-58.
[3] L. M. Dai, A. Patil, X. Y. Gong, Z. X. Guo, L. Q. Liu, Y. Liu and D. B. Zhu, *Chemphyschem* **2003**, *4*, 1150-1169.
[4] M. Terrones, *International Materials Reviews* **2004**, *49*, 325-377.
[5] M. L. Terranova, V. Sessa and M. Rossi, *Chemical Vapor Deposition* **2006**, *12*, 315-325.
[6] D. H. Robertson, D. W. Brenner and J. W. Mintmire, *Physical Review B* **1992**, *45*, 12592-12595.
[7] M. M. J. Treacy, T. W. Ebbesen and J. M. Gibson, *Nature* **1996**, *381*, 678-680.
[8] M. R. Falvo, G. J. Clary, R. M. Taylor, V. Chi, F. P. Brooks, S. Washburn and R. Superfine, *Nature* **1997**, *389*, 582-584.
[9] P. Kim, L. Shi, A. Majumdar and P. L. McEuen, *Physical Review Letters* **2001**, *87*.
[10] W. Yi, L. Lu, D. L. Zhang, Z. W. Pan and S. S. Xie, *Physical Review B* **1999**, *59*, R9015-R9018.
[11] a) P. Avouris, T. Hertel, R. Martel, T. Schmidt, H. R. Shea and R. E. Walkup, *Applied Surface Science* **1999**, *141*, 201-209; b) P. G. Collins and P. Avouris, *Scientific American* **2000**, *283*, 62-+.
[12] E. T. Thostenson, Z. F. Ren and T. W. Chou, *Composites Science and Technology* **2001**, *61*, 1899-1912.
[13] R. H. Baughman, A. A. Zakhidov and W. A. de Heer, *Science* **2002**, *297*, 787-792.
[14] J. W. Mintmire and C. T. White, *Carbon* **1995**, *33*, 893-902.
[15] R. S. Ruoff and D. C. Lorents in *Mechanical and thermal properties of carbon nanotubes, Vol. 33* **1995**, pp. 925-930.
[16] J. M. Bonard, T. Stockli, F. Maier, W. A. de Heer, A. Chatelain, J. P. Salvetat and L. Forro, *Physical Review Letters* **1998**, *81*, 1441-1444.
[17] A. G. Rinzler, J. H. Hafner, P. Nikolaev, L. Lou, S. G. Kim, D. Tomanek, P. Nordlander, D. T. Colbert and R. E. Smalley, *Science* **1995**, *269*, 1550-1553.
[18] E. Frackowiak and F. Beguin, *Carbon* **2002**, *40*, 1775-1787.
[19] G. L. Che, B. B. Lakshmi, E. R. Fisher and C. R. Martin, *Nature* **1998**, *393*, 346-349.
[20] C. Liu, Y. Y. Fan, M. Liu, H. T. Cong, H. M. Cheng and M. S. Dresselhaus, *Science* **1999**, *286*, 1127-1129.
[21] A. C. Dillon, K. M. Jones, T. A. Bekkedahl, C. H. Kiang, D. S. Bethune and M. J. Heben, *Nature* **1997**, *386*, 377-379.
[22] M. Terrones, R. Kamalakaran, T. Seeger and M. Ruhle, *Chemical Communications* **2000**, 2335-2336.
[23] H. J. Dai, J. H. Hafner, A. G. Rinzler, D. T. Colbert and R. E. Smalley, *Nature* **1996**, *384*, 147-150.
[24] S. S. Wong, A. T. Woolley, T. W. Odom, J. L. Huang, P. Kim, D. V. Vezenov and C. M. Lieber, *Applied Physics Letters* **1998**, *73*, 3465-3467.
[25] S. S. Wong, E. Joselevich, A. T. Woolley, C. L. Cheung and C. M. Lieber, *Nature* **1998**, *394*, 52-55.
[26] J. Kong, N. R. Franklin, C. W. Zhou, M. G. Chapline, S. Peng, K. J. Cho and H. J. Dai, *Science* **2000**, *287*, 622-625.
[27] O. K. Varghese, P. D. Kichambre, D. Gong, K. G. Ong, E. C. Dickey and C. A. Grimes, *Sensors and Actuators B-Chemical* **2001**, *81*, 32-41.
[28] S. Iijima, P. M. Ajayan and T. Ichihashi, *Physical Review Letters* **1992**, *69*, 3100-3103.
[29] S. Iijima, *Materials Science and Engineering B-Solid State Materials for Advanced Technology* **1993**, *19*, 172-180.
[30] M. Endo and H. W. Kroto, *Journal of Physical Chemistry* **1992**, *96*, 6941-6944.
[31] T. Guo, P. Nikolaev, A. Thess, D. T. Colbert and R. E. Smalley, *Chemical Physics Letters* **1995**, *243*, 49-54.
[32] P. M. Parthangal, R. E. Cavicchi and M. R. Zachariah, *Nanotechnology* **2007**, *18*.
[33] X. M. Liu, K. H. R. Baronian and A. J. Downard, *Carbon* **2009**, *47*, 500-506.
[34] R. T. K. Baker, M. A. Barber, P. S. Harris, F. S. Feates and R. J. Waite, *Journal of Catalysis* **1972**, *26*, 51-62.
[35] T. Baird, J. R. Fryer and B. Grant, *Carbon* **1974**, *12*, 591-602.
[36] R. T. K. Baker, P. S. Harris, R. B. Thomas and R. J. Waite, *Journal of Catalysis* **1973**, *30*, 86-95.
[37] X. Liu, K. H. R. Baronian and A. J. Downard, *Analytical Chemistry* **2008**, *80*, 8835-8839.

[38] J. S. Suh and J. S. Lee, *Applied Physics Letters* **1999**, *75*, 2047-2049.
[39] J. Li, C. Papadopoulos, J. M. Xu and M. Moskovits, *Applied Physics Letters* **1999**, *75*, 367-369.
[40] J. M. Xu, X. B. Zhang, C. Fei, T. Li, Y. Li, X. Y. Tao, Y. W. Wang and X. J. Wu, *Applied Surface Science* **2005**, *239*, 320-326.
[41] S. H. Jeong, H. Y. Hwang, S. K. Hwang and K. H. Lee, *Carbon* **2004**, *42*, 2073-2080.

Chapter 2: Experimental

2.1. Synthesis of Vertically Aligned Carbon Nanotubes on Si Chips

2.1.1. Preparation of Si Chips

N-type silicon (100) wafer was cut into 15x15 mm chips with a diamond tipped cutter. The wafer was first firmly mounted onto the cutter, and then the diamond tip was applied with pressure and the surface scored at 15 mm intervals in a grid pattern. The wafer was then broken into small square pieces along the scored lines. Any waste shards were discarded into a hazardous materials bin.

The Si chips were first sonicated in acetone for 30 min, and then were rinsed with acetone and absolute alcohol. Then the chips were dried under N_2 leaving a dry and clean surface for metal deposition. Piranha treatment was also used when the above treatment did not give a visibly clean surface. Piranha solution was prepared by adding 3 parts of conc. H_2SO_4 to 1 part of H_2O_2. This treatment is designed to remove any impurities from the Si surface. All work was carried out in glass, and caution was taken to not spill any as it is highly corrosive. The Si chips were immersed into the solution for approximately one minute, and then removed, rinsed with Milli-Q water and acetone, dried under N_2.

2.1.2. Metal Deposition on Si Chips

Two different metal deposition methods were used to prepare a Fe/Al catalyst layer on the Si chips for CNT growth.

In the first method, an Edwards 3000 e-beam evaporator was used to deposit 10 nm of Al followed by 10 nm of Fe on the Si chips.

In the second method, the catalytic layer was prepared from a solution containing ferric nitrate and aluminum nitrate[1]. Equal volume of 10 mM $Fe(NO_3)_3$ solution and 10 mM $Al(NO_3)_3$ solution were mixed together. Approximately 1 mL of the catalyst solution was applied to the Si chip surface and dried in air at approximately 60 ºC.

2.1.3. Carbon Nanotube Growth on Si Chips

2.1.3.1. Thermal Chemical Vapour Deposition Furnace Setup

A RADATHERM tube furnace equipped with a Eurotherm 2132 thermocouple and a Eurotherm 2216e temperature controller was used for carbon nanotube growth as shown in Fig 2.1. The working quartz tube had an inner diameter of 28 mm, and four gas lines Ar, H_2, C_2H_4 and Ar/H_2O were connected to the tube.

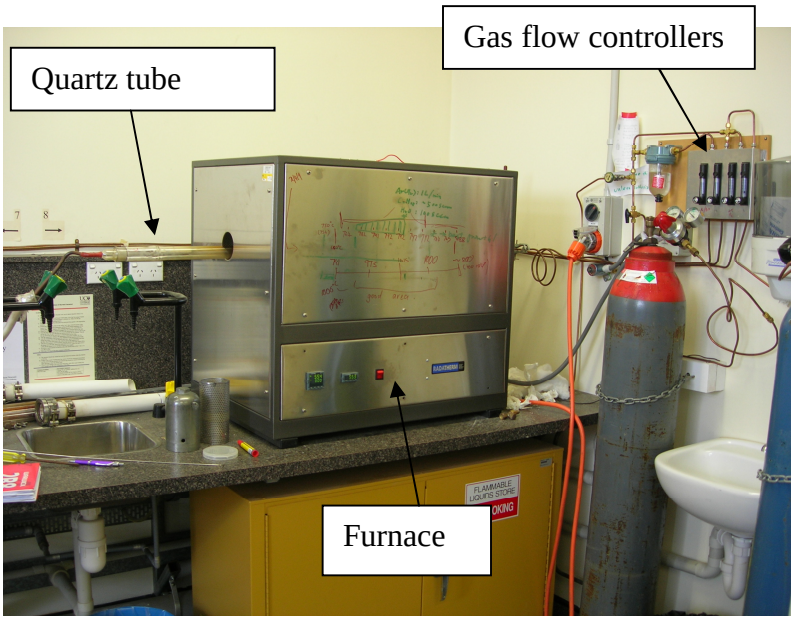

Fig 2.1 The thermal chemical vapour deposition furnace

2.1.3.2. Conditions and Procedure

The following procedure and conditions were used to grow vertically aligned carbon nanotubes (VACNTs) on the catalyst-loaded Si chips[2]. The Si chips were placed on a quartz boat, and then the boat was carefully inserted into the quartz tube. After the both ends of the tube were sealed, the Ar, H_2, C_2H_4 and Ar/H_2O gas lines were turned on for approximately 2 min to flush the gas lines and the tube, to remove O_2. Then, the Ar flow was maintained at 1200 sccm while other gas flows were stopped. After approximately 1 min, the furnace temperature was set to 750 ºC and once the furnace reached that temperature, the H_2 flow was set at 800 sccm for 30 min to reduce the catalyst. After 30 min, C_2H_4 flow was introduced at 750 ºC to grow carbon nanotubes with gas flows of C_2H_4: 400 sccm, Ar: 1000 sccm and H_2: 800 sccm. At the same time, a small amount of water vapour was carried into the tube by bubbling 50 sccm Ar through water. After 15 min growth time, the Ar flow was maintained at 1000

sccm and other flows were turned off, and the furnace temperature was set to 25 °C. The furnace was cooled to below 200 °C under the Ar flow before removing the samples from the furnace.

2.2. Synthesis of Carbon Nanotubes using PAA Templates

2.2.1. Preparation of PAA Templates

2.2.1.1. Anodization Cell Setup

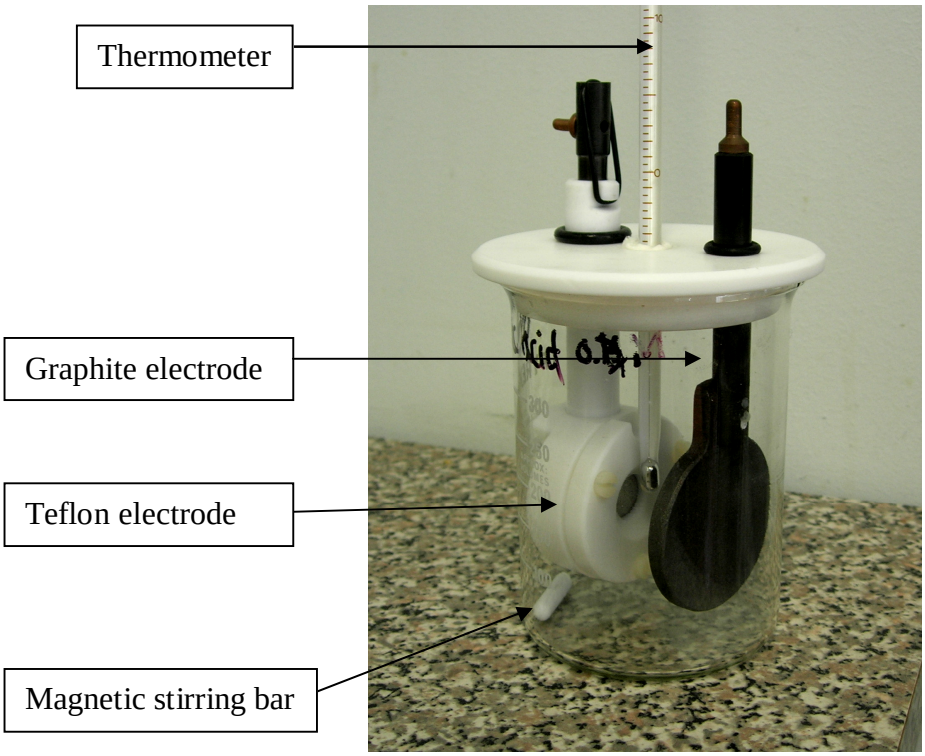

Fig 2.2 The anodization cell setup.

The anodization of Al foils was carried out in the 2 electrode cell as shown in Fig 2.2. A teflon cap holding two electrodes and a thermometer is placed on a 400 mL beaker containing a magnetic stirring bar. The teflon electrode was used as an anode, and the graphite electrode was used as the cathode. The cell cap and electrodes were fabricated in-house.

Fig 2.3 shows the components of the teflon electrode. A graphite rod fitted with a brass screw makes contact with a graphite disc which sits on the teflon base. Three nylon screws and two O-rings on the front plate seal the electrode and prevent leakage of solution. To assemble the electrode, a disc of Al is first placed on the graphite disc, and the assembly is sealed with the front plate. Then the graphite rod is inserted into the teflon tube to contact the graphite disc. A rubber band secures the graphite rod and ensures contact with the graphite disc in the base of the assembly (Fig 2.2).

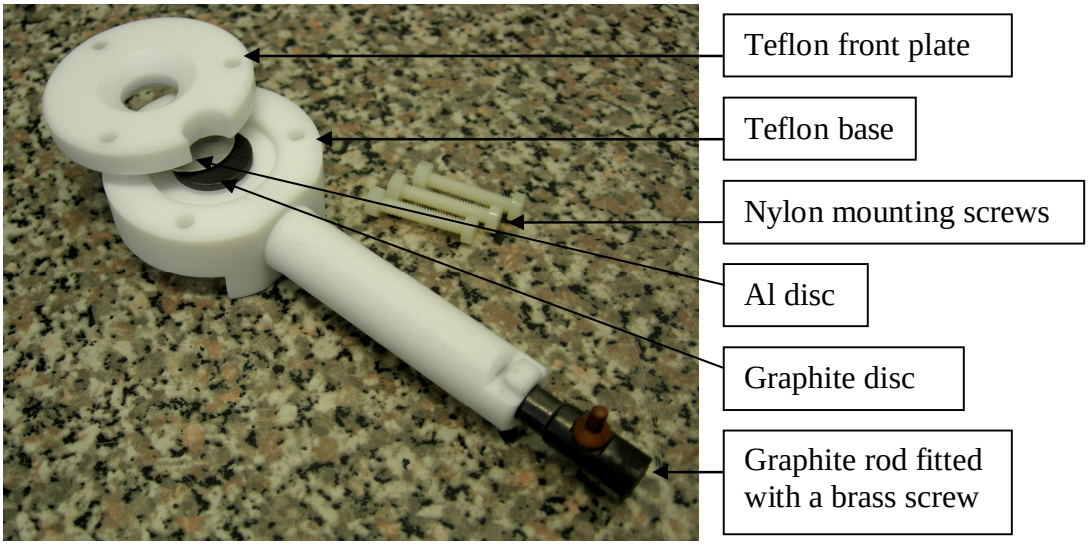

Fig 2.3 Components of the teflon electrode.

2.2.1.2. Sample Pretreatment

A piece of 0.5 mm thick, annealed, 99.9995% pure Al foil provided by Puratronic was cut into discs of approximately 2 cm diameter. The following simple pretreatment was used[3]. The Al discs were degreased in acetone under sonication over 30 min, and then were rinsed with distilled water (DW), and dried under N_2.

For some experiments, electropolishing was also used after the simple pretreatment to study its effect on the Al surface morphology. The following electropolishing process was used[4]. After the simple pretreatment, the Al samples were electropolished in a solution containing $HClO_4$ (60%) and ethanol (1:4 v/v) at ~10 °C and 20 V for different time periods using the anodization cell (Fig 2.2) as described earlier. After electropolishing, the samples were rinsed thoroughly with DW and then dried under N_2.

2.2.1.3. Anodization of Aluminium

A two-step anodization method was used to prepare porous anodic alumina (PAA) templates[5],[6]. A pre-treated Al disc was mounted in the teflon electrode holder (Fig 2.3) as described earlier. The Al anode and graphite cathode were placed in the 400 mL beaker containing 200 mL of 0.4 M oxalic acid and a magnetic stirring bar. A thermometer was positioned between the two electrodes. The beaker was then placed in a water bath on a stirrer. In order to control the cell temperature at a selected value between 10 °C to 25 °C, a stirring rate of 1000 rpm was used and a certain amount of ice was added into the water bath. Once the cell temperature was maintained at the

selected value, the two electrodes were connected to a 30 V DC power supply and a constant 30 V voltage was applied. After a selected anodization time, the Al disc was removed from the anode, rinsed with DW, and then was immersed in a solution containing 10 mL of 0.8 M H_3PO_4 and 10 mL of 0.2 M H_2CrO_4 for 30 min to 60 min at approximately 65 ºC. This treatment dissolves the PAA membrane formed during the anodization process. Then the Al disc was rinsed with DW and dried under N_2. A second anodization was carried out under the same conditions as described above.

2.2.2. Electrochemical Deposition of Cobalt

2.2.2.1. Electrodeposition Cell Setup

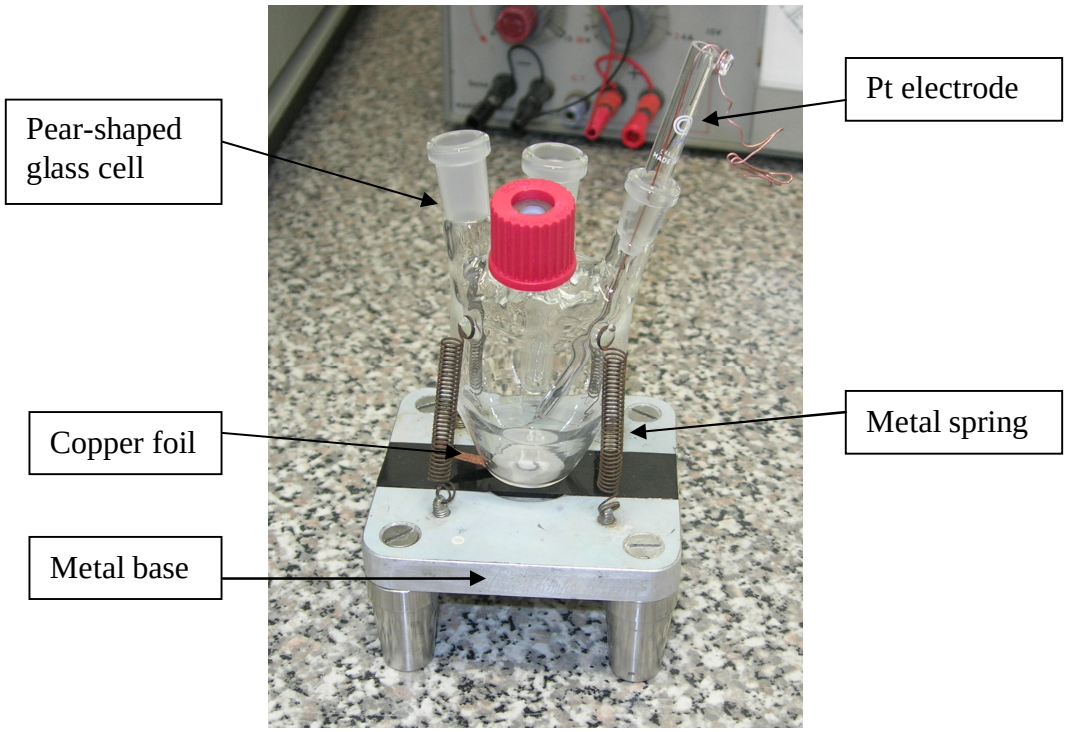

Fig 2.4 Cell setup for electrodeposition of cobalt

Electrodeposition of cobalt was carried out in the 2 electrode cell as shown in Fig 2.4. A PAA sample is positioned between the metal base plate and the pear-shaped glass cell with a hole of approximately 30 mm diameter in the base. A viton O-ring between sample surface and cell base, along with four metal springs attached to the four corners of the cell stabilise the setup and provide a seal to avoid leakage of solution. A copper foil lies underneath the PAA sample to allow connection to the working electrode. A Pt electrode was used as the counter electrode.

2.2.2.2. Barrier Layer Thinning

For AC electrodeposition, barrier layer thinning of PAA membranes prior to electrodepostion is applied in order to obtain uniform filling of the pores[7]. Three barrier layer thinning processes were examined. In the first method, a gradual voltage drop at the end of the 2nd anodization was used. The anodizing voltage was gradually dropped from 30 V to a selected value, and then was kept at the selected voltage for 3 min in order to achieve equilibrium at the barrier layer[8]. In the second method, a chemical etching process was used. PPA templates were immersed in 0.1 M H_3PO_4 at approximately 30 °C for 1 h[9]. In the final method, a combination of the above two methods was used. The barrier layer was first thinned by dropping anodizing voltage at the end of the 2nd anodization, and then the PAA templates were chemically etched to further thin the barrier layer[10].

2.2.2.3. Electrodeposition Conditions and Procedure

After barrier layer thinning, PAA templates were rinsed with DW and then was immersed in a solution containing 240 g/L $CoSO_4$ and 40 g/L H_3BO_3[9] overnight on an orbital shaker in order to allow enough time for Co^{2+} ions diffusion into the pores. However, some PAA samples were soaked in the solution for only 15 min. This solution was later used as the electrolyte for electrodeposition of Co. After rinsing the sample with DW (in order to remove any Co^{2+} ions that were not inside of the pores), the sample was mounted in the electrodeposition cell as shown in Fig 2.4. The cell was then connected to an EG&G PARC 273A potentiostat, which was connected to an EG&G PARC MODEL 175 waveform generator as shown in Fig 2.5.

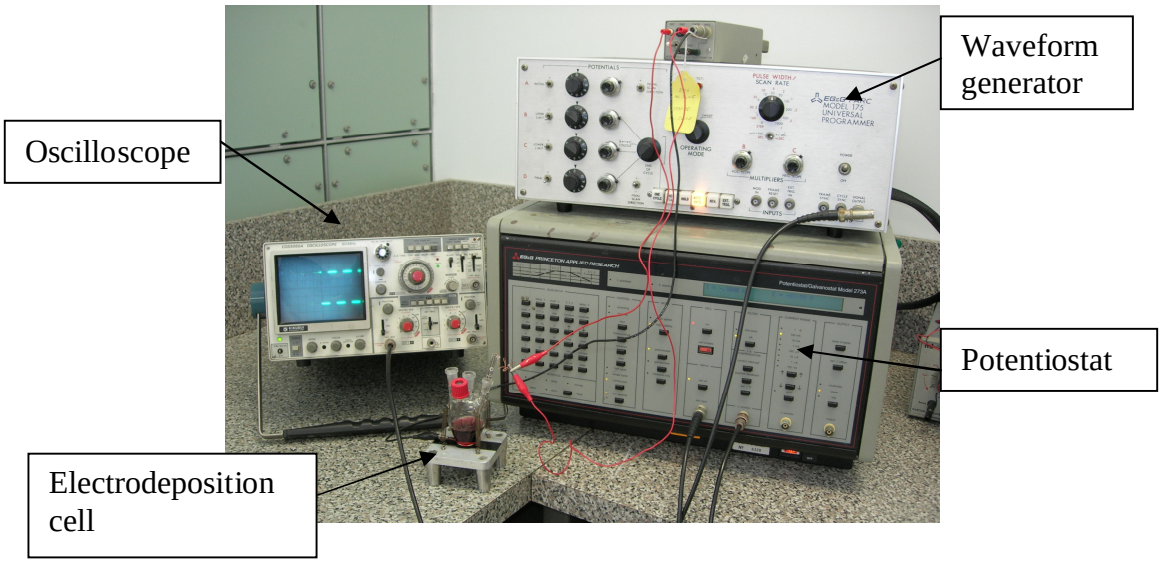

Fig 2.5 The eletrodeposition setup

10 V_{peak}, 100 Hz square waveform with reductive/oxidative (5 ms/5 ms) pulse polarity was programmed using the waveform generator[8],[9], and was monitored by an

oscilloscope. The deposition duration was varied between 10 s and 30 min. The sample was removed from the cell after electrodeposition, and was rinsed, then immersed in DW overnight on the orbital shaker in order to wash off any Co^{2+} ions from the sample membrane. The sample was then dried by N_2 and was ready for CNT growth.

2.2.3. Carbon Nanotube Growth on PAA Templates

The same furnace setup (Fig 2.1) and procedure as described earlier were used for growing CNTs from the Co-loaded PAA templates. However the conditions were changed.

The samples were reduced at 500 ºC for 1 h with gas flows of Ar: 1000 sccm and H_2: 800 sccm. Then, CNTs were grown at 600 ºC for 10 min with gas flows of Ar: 1000 sccm, H_2: < 100 sccm and C_2H_4: 400 sccm[11]. For some experiments, 25 sccm water vapor was also introduced into the tube furnace during the CNT growth.

2.3. SEM Measurements and Sample Preparation

Field emission scanning electron mircroscope (FESEM) images of prepared CNTs and PAA templates were obtained using a Jeol JSM 7000 FESEM, operating with the accelerating voltage ranging from 5 kV to 10 kV and working distance ranging from 4 mm to 15 mm. A few SEM images of prepared CNTs were obtained using a Leica S 440 SEM, operating with the accelerating voltage at 10 kV, I filament of 2.72 A and

working distance of 14 mm. Optimisation of the images was carried out by adjusting the brightness and contrast.

To prepare a cross-section of a PAA sample for FESEM imaging, a PAA sample was partially immersed in a solution containing 0.51 g of $CuCl_2$, 25 mL of distilled water and 5 mL of HCl (38%) in order to remove the Al substrate. Since the PAA membrane does not dissolve in this solution, after a certain reaction time (20-60 min), the Al substrate can be completely removed, leaving a transparent PAA membrane. During this detaching process, the unsupported PAA membrane was snapped off the sample, leaving a clean cross-section of PAA membrane.

2.4. Chemicals

Chemical	**Formula**	**Supplier**
Aluminium foils (99.9995%)	Al	Puratronic
Sulphuric Acid (98%)	H_2SO_4	BDH
Hydrogen Peroxide (50%)	H_2O_2	BDH
Aluminum Nitrate (CP)	$Al(NO_3)_3 \cdot 9H_2O$	BDH
Ferric Nitrate (CP)	$Fe(NO_3)_3 \cdot 9H_2O$	BDH
Perchloric Acid (60%)	$HClO_4$	BDH
Hydrochloric Acid (38%)	HCl	Riedel-de Haen Ag Seelze-Hannover
Oxalic Acid (AR)	$H_2C_2O_4$	BDH
Phosphoric Acid (90%)	H_3PO_4	BDH
Boric Acid (CP)	H_3BO_3	BDH
Chromium Trioxide (CP)	CrO_3	BDH
Cupric Dichloride (AR)	$CuCl_2 \cdot 2H_2O$	BDH
Cobalt Sulfate heptahydrate (CP)	$CoSO_4 \cdot 7H_2O$	BDH
Absolute Alcohol	C_2H_6O	BDH
Ethanol	C_2H_6O	BDH
Acetone	C_3H_6O	BDH
Nitrogen gas	N_2	BOC
Hydrogen gas	H_2	BOC
Ethylene	C_2H_4	BOC
Argon gas	Ar	SGS Limited / BOC

References

[1] P. M. Parthangal, R. E. Cavicchi and M. R. Zachariah, *Nanotechnology* **2007**, *18*.
[2] X. M. Liu, K. H. R. Baronian and A. J. Downard, *Carbon* **2009**, *47*, 500-506.
[3] J. H. Yuan, F. Y. He, D. C. Sun and X. H. Xia, *Chemistry of Materials* **2004**, *16*, 1841-1844.
[4] A. Rauf, M. Mehmood, M. A. Rasheed and M. Aslam, *Journal of Solid State Electrochemistry* **2009**, *13*, 321-332.
[5] H. Masuda and K. Fukuda, *Science* **1995**, *268*, 1466-1468.
[6] Y. C. Zhao, M. Chen, Y. N. Zhang, T. Xu and W. M. Liu, *Materials Letters* **2005**, *59*, 40-43.
[7] K. Nielsch, F. Muller, A. P. Li and U. Gosele, *Advanced Materials* **2000**, *12*, 582-586.
[8] N. J. Gerein and J. A. Haber, *Journal of Physical Chemistry B* **2005**, *109*, 17372-17385.
[9] J. Li, M. Moskovits and T. L. Haslett, *Chemistry of Materials* **1998**, *10*, 1963-1967.
[10] S. H. Jeong, O. J. Lee, K. H. Lee, S. H. Oh and C. G. Park, *Chemistry of Materials* **2002**, *14*, 4003-4005.
[11] S. H. Jeong, H. Y. Hwang, S. K. Hwang and K. H. Lee, *Carbon* **2004**, *42*, 2073-2080.

Chapter 3: Porous Anodic Alumina Templates

3.1 Introduction

Porous anodic alumina (PAA) membranes with an ordered nanopore structure have received a great deal of attention in the development of various nanodevices[1],[2]. PAA membranes are known to have vertically aligned nanopores with high density and high aspect ratio as shown in Fig 3.1. PAA membranes have been widely used as templates in fabricating nanostructures such as carbon nanotubes[3] and metal nanowires[4] due to their unique structural properties.

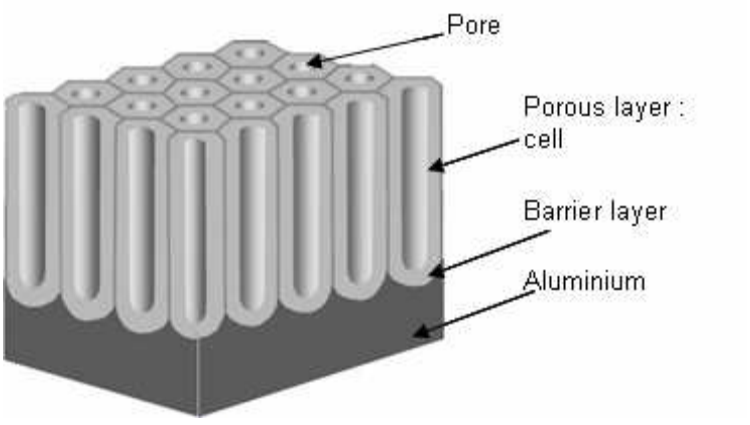

Fig 3.1 A schematic drawing of an ideal PAA membrane.
(Adopted from reference 20)

3.1.1 The Mechanism of Pore Formation

Two types of alumina layer normally form during anodization of aluminium depending on the properties of the electrolyte employed[5]. A nonporous planar layer forms in a near-neutral electrolyte, while a porous layer forms in acidic electrolytes such as H_2SO_4, $H_2C_2O_4$ (oxalic acid) and H_3PO_4. It has been widely accepted that two basic chemical processes take place during the anodization of aluminium: dissolution of Al_2O_3 at the electrolyte/oxide interface and oxidation of aluminium at the oxide/metal interface. Fig 3.2 illustrates the pore formation procedure during the anodization.

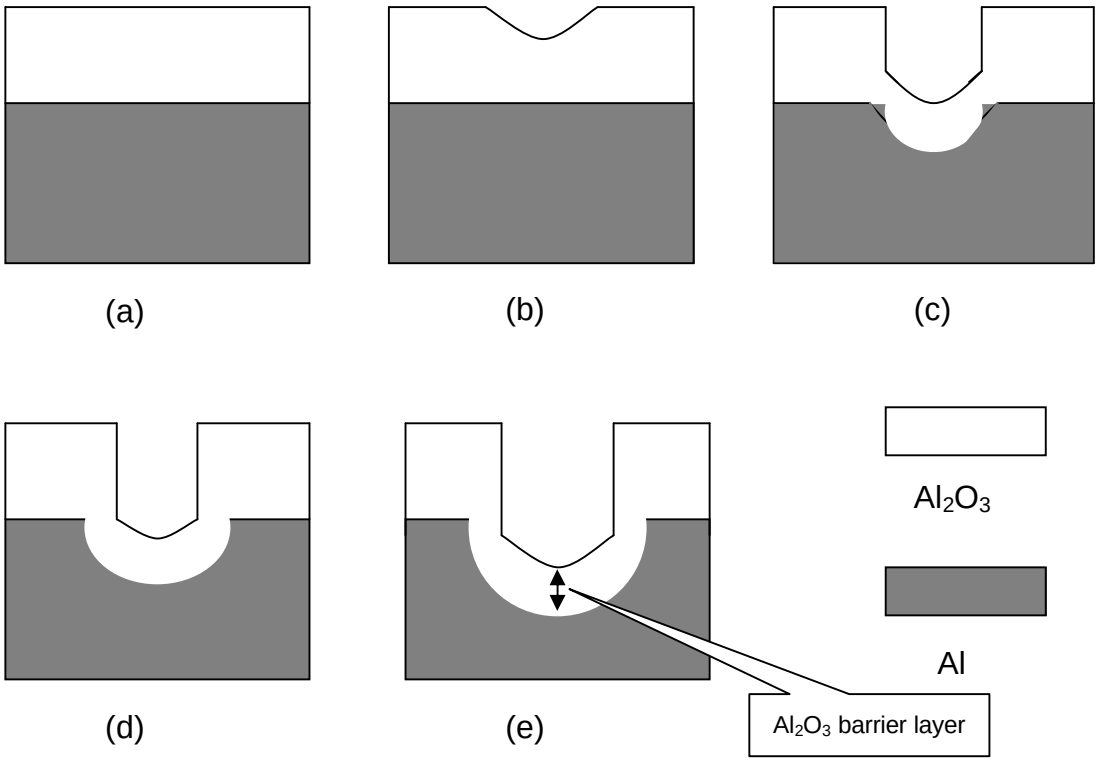

Fig 3.2 A schematic diagram of the pore formation. (a) Formation of a planar Al_2O_3 layer with a uniform thickness, (b) pore nucleation on the Al_2O_3 surface, (c) initial pore development, (d) and (e) further pore growth.

An Al_2O_3 layer forms on the starting Al surface at the beginning of the anodization as shown in Fig 3.2a. The following reactions shown in equations (1)-(4) take place during the Al_2O_3 formation[6],[7]:

(1) $Al\,(s) \rightarrow Al^{3+}\,(aq) + 3e^-$

(2) A water-splitting reaction gives O^{2-} and OH^-

(3) $2Al^{3+}\,(aq) + 3O^{2-} \rightarrow Al_2O_3\,(s)$

(4) $2Al^{3+}\,(aq) + 3OH^- \rightarrow Al_2O_3\,(s) + 3H^+$

Al^{3+} ions form at the metal/oxide interface and migrate into the oxide layer, while the oxygen containing ions (O^{2-} and OH^-) migrate within the oxide layer from the oxide/electrolyte interface toward the metal/oxide interface under the electric field to form Al_2O_3[7].

Field-assisted H^+ attacking on the Al_2O_3 layer results in local dissolution of the Al_2O_3 layer, and the local heat resulting from the high resistance of the Al_2O_3 layer promotes this dissolution process as shown in equation (5)[8],[9].

(5) $Al_2O_3\,(s) + 6H^+\,(aq) \rightarrow 2Al^{3+}\,(aq) + 3H_2O\,(l)$

This results in pore nuclei formation on the Al_2O_3 surface as shown in Fig 3.2b. If the H^+ concentration is decreased, then this attack will be slow or stop and a nonporous

Al_2O_3 layer will form instead[9]. This explains why porous alumina membranes can only be obtained from acidic electrolytes. After the initial pore development (Fig 3.2c), when the formation rate of Al_2O_3 is equal to the local dissolution rate of the oxide at the bottom of the pores, the thickness of the Al_2O_3 barrier layer reaches a constant value (Fig 3.2d). Further pore growth will increase the pore size as shown in Fig 3.2e [7].

3.1.2 The Self-Ordering of Pore Arrays

Masuda *et al.* [10] first proposed a two-step anodization process to achieve a highly ordered pore arrangement over a large area. In this method, the dimples formed on aluminum base after removal of the PAA membrane formed during the first anodization step work as the initial sites for the pore growth in the second anodization step. A schematic diagram of this method is shown in Fig 3.3.

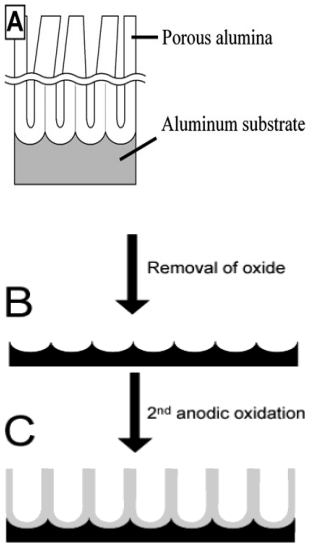

Fig 3.3 A schematic diagram of the two-step anodzation process.
(Adopted from reference 8)

The pores initiate at almost random positions on the oxide surface. The pore arrangement is disordered and the pore arrays are not aligned. However, the pores are getting ordered by self-adjusting as they develop during the 1st anodization. Therefore, vertically aligned pore arrays and ordered pore arrangement can be obtained at the bottom of the membrane as shown in Fig 3.3A. After the removal of the Al_2O_3 membrane formed from the 1st anodization by dissolution in an acid mixture, the leftover surface consists of ordered concave patterns as shown in Fig 3.3B, which act as a template for the 2nd anodization. Vertically aligned and well ordered pore arrays can be obtained during the 2nd anodization under the same conditions as for the 1st anodization [6, 8, 11] (Fig 3.3C and Fig 3.4).

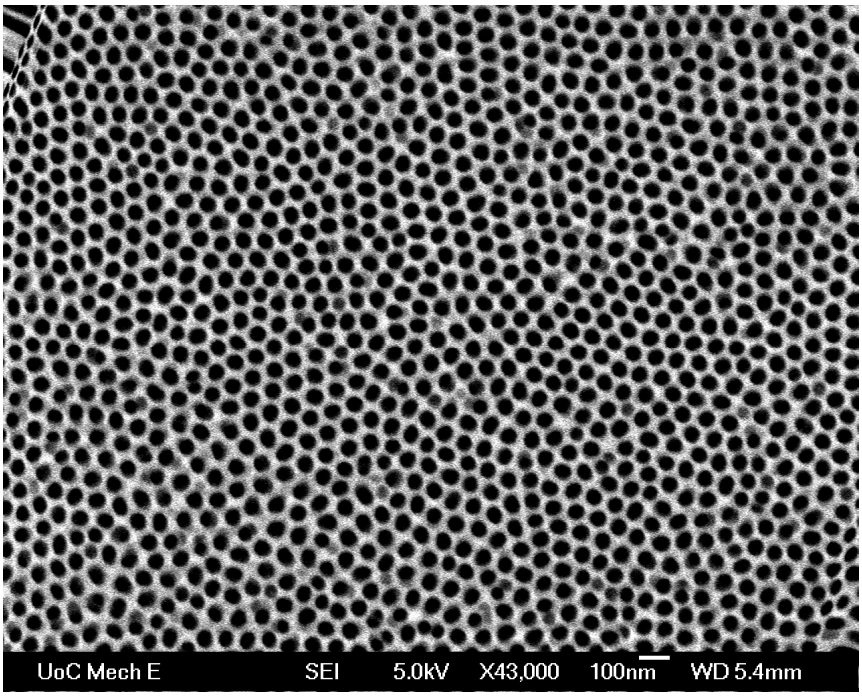

Fig 3.4 FESEM image of a highly ordered porous anodic alumina membrane fabricated using the two-step anodization method.

The mechanism for the self-ordering of pores in PAA is generally believed to be based on mechanical stress[6],[7]. Jessensky *et al.*[6] suggested that mechanical stress associated with the expansion of the aluminium during oxide formation was the cause of repulsive forces between neighbouring pores during the anodization process, and this was the driving force for the self-ordering process of the pores.

3.1.3 The Kinetics of the Pore Formation

The pore formation occurs in several stages that can be observed from the characteristic behaviour of current density *vs* anodizing time, as shown in Fig 3.5.

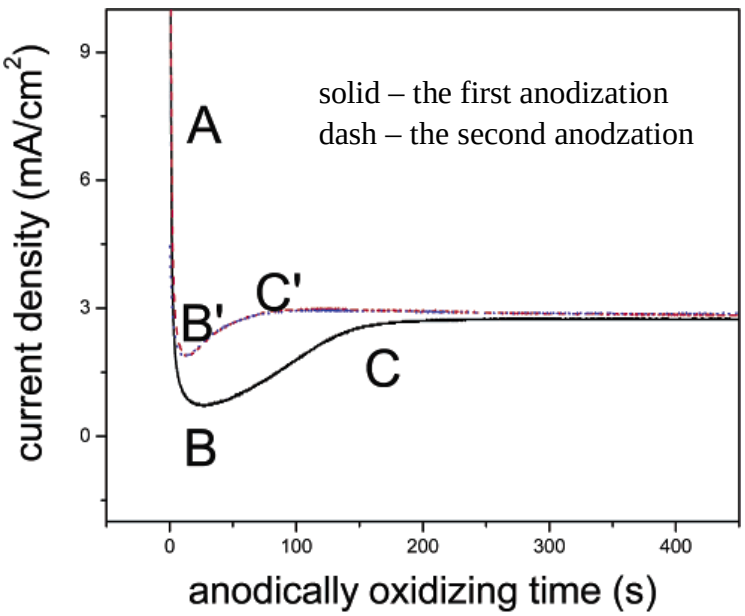

Fig 3.5 Current density acts as a function of time during the anodization processes. (Adopted from reference 8)

In the first region A, a nonporous planar Al_2O_3 layer forms immediately when the anodization starts. With the formation of the Al_2O_3 layer, resistance of the Al anode increases considerably, resulting in a sharp decrease in current density (A à B or A à B'). This process corresponds to Fig 3.2a.

The local dissolution of the Al_2O_3 layer results in a decrease in the thickness of the Al_2O_3 layer, as shown in Fig 3.2a à b à c. This is indicated by an increase in the current density (B à C or B' à C').

After a certain pore growth time, the thickness of the barrier layer reaches a constant value (Fig 3.2d and e) as indicated by the steady state current (after C or C'). At this point, the formation rate of the oxide is equal to the local dissolution rate of the oxide at the bottom of the pores.

There are several important differences between the results observed in the first and second anodization in Fig 3.5. For the second anodization, the times for reaching the lowest and constant current density are shorter than those for the first anodization. In addition, the lowest current density is higher for the second anodization than for the first anodization.

The longer time for reaching the steady-state condition in the first anodization is simply due to the fact that at the beginning the porous structure is not formed[8].

Therefore, the time for pore nucleation and growth during the first anodization (Fig 3.5, points B and C) is longer than that in the second anodization process (points B' and C'), in which the pore patterning was already formed from the first anodization. Obviously, the time for reaching the lowest current density in the second oxidation process is also shorter.

Under a constant anodizing voltage, the observed larger current density in the second anodizaion step (B' and C' in Fig 3.5) is owing to the dimpled surface area left by the dissolution of previous porous structure[8].

3.1.4 The Effects of Anodizing Conditions on Pore Formation

The pore characteristics in terms of pore diameter, interpore distance, membrane thickness and porosity are controlled by the processing parameters such as anodizing voltage, temperature, duration, type and concentration of the electrolyte[7],[12],[13],[14].

Table 3.1 summarizes the pore diameter, interpore distance and porosity can be obtained by using three most commonly used electrolytes under standard anodizing conditions.

Table 3.1 Effects of anodization conditions on the structural properties of PAA membranes.

Electrolyte/Voltage	**Pore diameter (nm)**	**Interpore distance (nm)**	**Porosity**
0.3M H_2SO_4/25V	~24	~66	~12%
0.3M $(COOH)_2$/40V	~31	~105	~8%
0.1M H_3PO_4/195V	~158	~500	~9%

The work described in this chapter investigated effects of the Al surface morphology and anodization conditions on the ordering of the pore arrangement of PAA membranes. The purpose of these studies was to be able to prepare well-ordered PAA templates for synthesis of carbon nanotubes described in the following chapter.

3.2 Results and Discussion

3.2.1 Method Development

It has been reported that the pore structure of PAA can be affected by Al surface morphology, and that ordered pore arrays can be obtained by one-step anodization on electropolished Al foils as an alternative to two-step anodization on non-electropolished Al foils[15]. Series of experiments were carried out in order to find a suitable method for making well-ordered PAA templates using the experimental setup as described in Chapter 2.

3.2.1.1 One-step Anodization on Electropolished Aluminium Foils

A piece of 0.5 mm thick, annealed, 99.9995% pure Al foil was cut into discs of approximately 2 cm diameter. The Al discs were first degreased in acetone under sonication over 30 min, and then were rinsed with distilled water (DW), and dried under N_2.

Electropolishing was then carried out using the anodization cell as described in Chapter 2, in a solution containing $HClO_4$(60%) and ethanol (1:4 v/v) at ~10 ℃ and 20 V for different time periods as shown in Table 3.2 [16],[17].

Table 3.2 Experimental conditions used for one-step anodization on electropolished Al samples

Sample	Electropolishing	One-step Anodization
Sample-1&1’	20 V, ~10 ℃, 300 s	-
Sample-2	20 V, ~10 ℃, 120 s	-
Sample-3	20 V, ~10 ℃, 10 s	30 V, 0.4 M $H_2C_2O_4$, 20 ± 2 ℃, 1000 rpm, 6h

Note: 1’ is a duplicate of 1

Although 5 min electropolished Al samples had a mirror-like surface, holes were found on the samples. Similar to samples 1&1’, samples 2 also had holes on its mirror-like surface. The damage on these samples probably results from leakage of

the electrolyte into the teflon anode, as the electrolyte is very corrosive to the mounting screws and the O-rings (Fig 2.4). Therefore, a much shorter polishing time was used, and samples 3 with 10 s electropolishing had a relatively shiny surface compared to samples 1&1' and 2 without any visible damages. Since samples 1&1' and 2 were damaged during the electropolishing process, only sample 3 was anodized under the conditions shown in Table 3.2.

Field emission scanning electron microscopy (FESEM) image of sample 3 was taken after 6 h anodization and is shown in Fig 3.6.

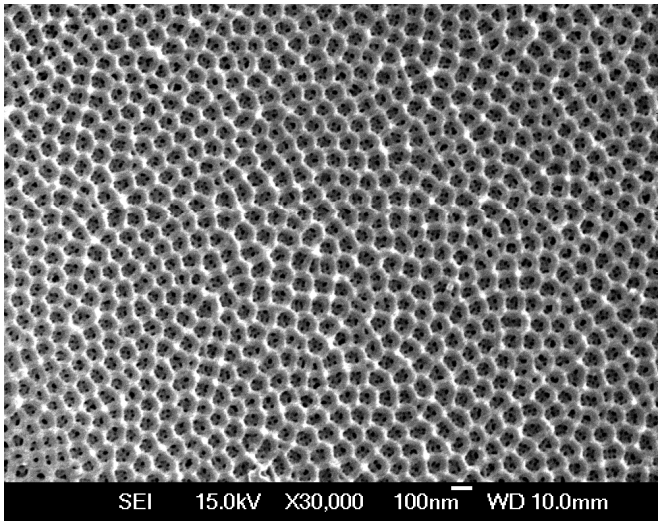

Fig 3.6 FESEM image of top view of sample 3

An ordered pore arrangement was obtained on sample 3 as shown in Fig 3.6. This result is expected as the electropolishing not only provides a very clean and flat surface, but also yields nanoscale morphology such as nanopits on the Al surface (Fig

3.7) that can facilitate the pore nucleation during the initial anodization[15],[17],[18],[19].

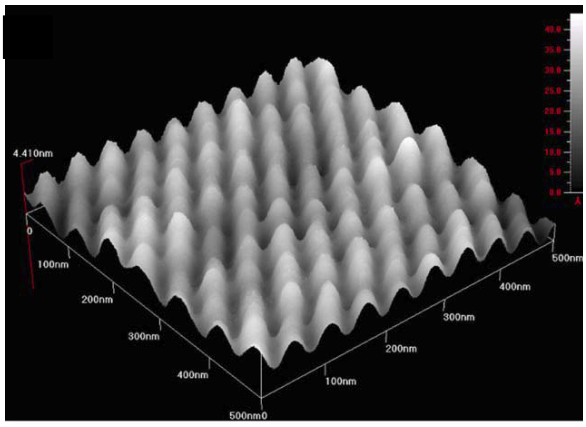

Fig 3.7 Typical AFM image of aluminum surfaces after electropolishing in a perchloric acid–alcohol solution at 20 V. (Adopted from reference 17)

3.2.1.2 Two-step Anodization on Non-electropolished Aluminium Foils

Four PAA samples were prepared using the two-step anodization method. The four Al samples did the same pre-treatment as for samples 1&1', 2 and 3, but were not electropolished. The anodizing conditions for all four samples were kept the same except for the anodizing temperature, which was varied between each sample as shown in Table 3.3.

Table 3.3 Experimental conditions used for two-step anodization on non-electropolished Al samples

Sample	**1st Anodization**	**2nd Anodization**
Sample 4	30 V, 0.4 M $H_2C_2O_4$, 13 ± 2 °C, 1000 rpm, 6h	30 V, 0.4 M $H_2C_2O_4$, 13 ± 2 °C, 1000 rpm, 4h
Sample 5	30 V, 0.4 M $H_2C_2O_4$, 16 ± 2 °C, 1000 rpm, 6h	30 V, 0.4 M $H_2C_2O_4$, 16 ± 2 °C, 1000 rpm, 4h
Sample 6	30 V, 0.4 M $H_2C_2O_4$, 18 ± 2 °C, 1000 rpm, 6h	30 V, 0.4 M $H_2C_2O_4$, 18 ± 2 °C, 1000 rpm, 4h
Sample 7	30 V, 0.4 M $H_2C_2O_4$, 20 ± 2 °C, 1000 rpm, 6h	30 V, 0.4 M $H_2C_2O_4$, 20 ± 2 °C, 1000 rpm, 4h

The four Al samples were first degreased in acetone under sonication over 30 min, and then were rinsed with DW, and dried under N_2. After the 1st anodization, the samples were immersed in a solution containing 0.8 M H_3PO_4 and 0.2 M H_2CrO_4 at approximately 65 °C for 1 h to remove the PAA membrane formed during the 1st anodization. They were rinsed and dried, and the 2nd anodization was carried out under the same conditions as for the 1st anodization for 4 h. FESEM images of these samples are shown in Fig 3.8.

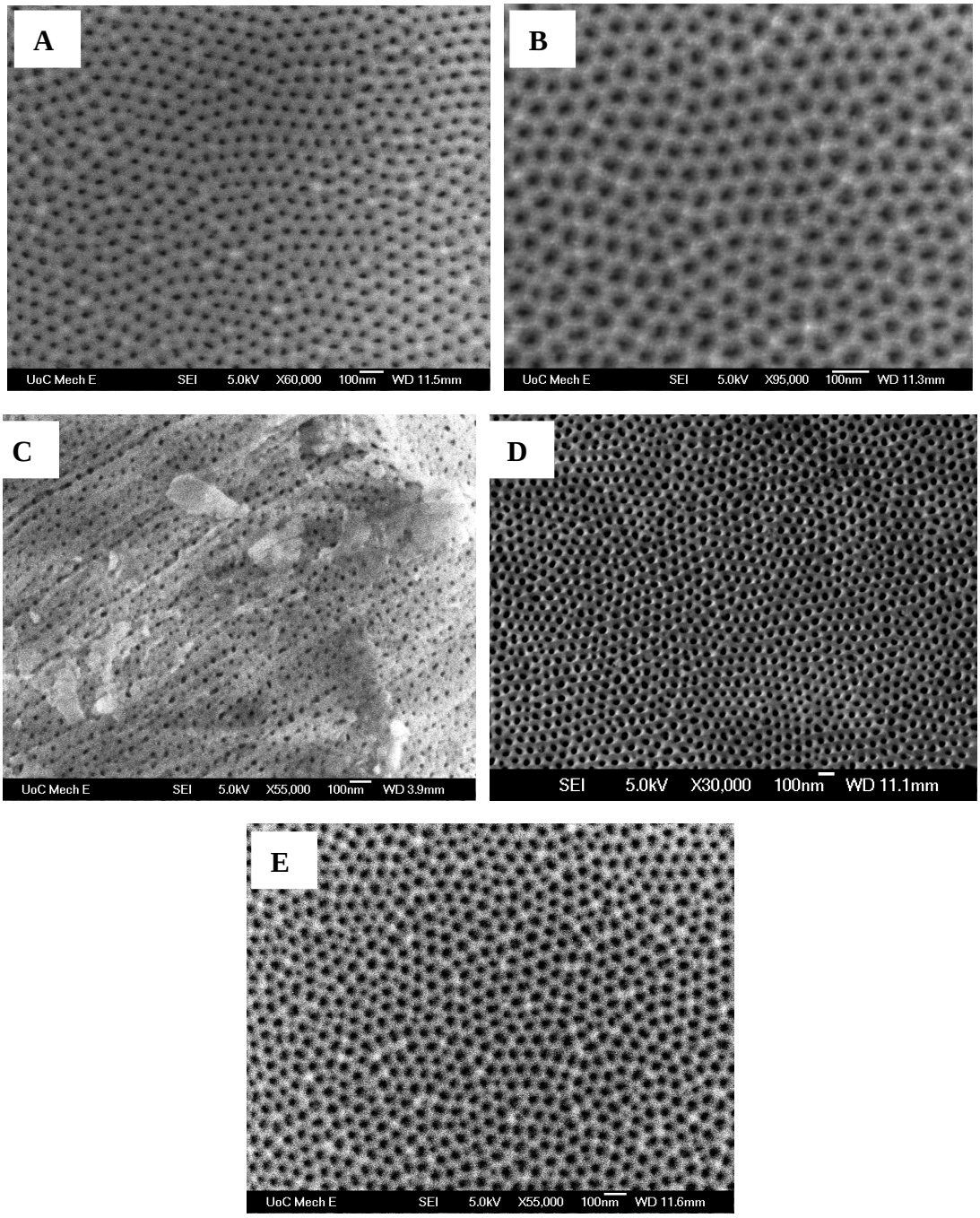

Fig 3.8 FESEM images of top view of (A) sample 4 after the 2nd anodization, (B) sample 6 after the 2nd anodization, (C) sample 5 after the 1st anodization, (D) sample 5 after the 2nd anodization, (E) sample 7 after the 2nd anodization.

For sample 5, a rough surface with disordered pores was obtained after the 1st anodization (Fig 3.8C). However, after the 2nd anodization, a smooth surface with ordered pores was obtained as expected (Fig 3.8D). Fig 3.8 A, B and E also show ordered pore arrangement for samples 4, 6, and 7 respectively after the 2nd anodization. From Fig 3.6 and Fig 3.8A-E, it is concluded that the pore size was widened through use of a higher anodization temperature (pore size: sample 4 < sample 5 < sample 6 <sample 7 < sample 3). This is not surprising because electrochemical reactions will proceed more quickly at higher temperature. However, sample 3 has larger pore size than sample 7 at the same anodizing temperature. This is probably due to a longer anodizing duration (6 h for sample 3 but 4 h for sample 7). However, it is difficult to tell whether the temperature difference has any effects on the pore arrangement from these FESEM images.

3.2.1.3. Two-step Anodization on Electropolished Aluminium Foils

One experiment was carried out using the two-step anodization method on an electropolished Al sample as shown in Table 3.4.

Table 3.4 Experimental condition for two-step anodization on electropolished Al sample

Sample	**Electropolishing**	**1st anodization**	**2nd anodization**
Sample 8	20 V, a solution of $HClO_4$ and ethanol (1:4 v/v), ~10 °C, 10 s	30 V, 0.4 M $H_2C_2O_4$, 13 ± 2 °C, 1000 rpm, 6h	30 V, 0.4 M $H_2C_2O_4$, 13 ± 2 °C, 1000 rpm, 4h

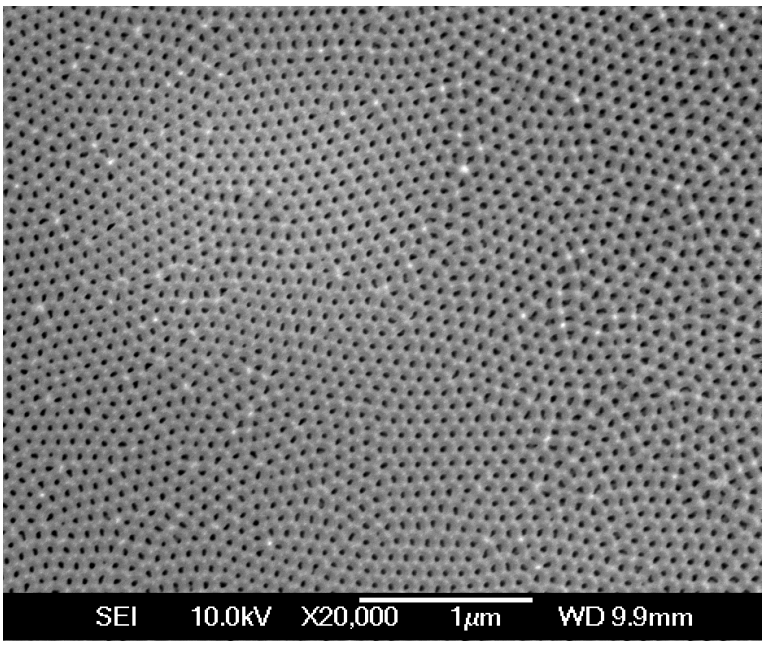

Fig 3.9 FESEM image of top view of sample 8.

As shown in the FESEM image of Fig 3.9, a highly ordered pore arrangement was obtained as expected. Since, electropolishing can provide a very smooth starting surface and ordered nanopits (Fig 3.7) on the Al surface, after removal of the oxide formed from the 1st anodization of 6 h, a well-ordered concave pattern is expected to be left on the remaining surface and it acts as nucleation sites for the pore formation during the 2nd anodization. Further self-ordering during the 2nd anodization of 4 h

leads to a highly ordered pore arrangement as shown in Fig 3.9.

Figs 3.6, 3.8 and 3.9 have showed the effect of surface morphology on the pore structure. Under the same processing conditions, the better (in terms of cleanness, smoothness, ordered nanopattern) the Al surface morphology, the more ordered pore structure can be obtained.

By examining the above three approaches, the two-step anodization on non-electropolished Al sample was used simply because the electrolyte solution used for electropolishing is very corrosive to the electrode mounting screws and the O-rings.

3.2.2 Effect of the Anodization Duration on the Pore Arrangement and Membrane Thickness

To study the effect of the anodizing duration on the pore arrangement, the following experiments were carried out as shown in Table 3.5.

Table 3.5 Samples prepared for investigating the effect of anodization time on pore arrangement.

Sample	Pretreatment	Anodizing conditions	Anodizing duration (1st/2nd)
9	Degreased in acetone under sonication over 30 min	30 V, 0.4M $H_2C_2O_4$ ~16 •C, 1000 rpm	1h/1h
10			2h/1h
11			4h/30min
12			4h/1h
13			4h/2h

The FESEM images of the prepared samples are shown in Figs 3.10-3.14. It is found that sample 9 with the shortest 1st anodization duration (Fig 3.10) does not have an ordered pore arrangement. It is assumed that for a 1st anodization of 1 h, pore ordering does not occur. Hence, after removal of the oxide membrane, the leftover surface does not have an ordered dimple pattern needed for the initiation of the 2nd anodization. Samples 10-13 with longer 1st anodization duration have an ordered pore arrangement as shown in Figs 3.11-3.14. For samples 11, 12 and 13, the uniformity of the pore diameter and the ordering of the pore arrangement are improved slightly with increasing the 2nd anodization duration. In comparison with samples 11, 12 and 13, sample 10 has a similar ordering of the pore arrangement with slightly smaller pore diameter. These results indicate that the ordering of the pore arrangement strongly depends on the 1st anodization duration (within 2 h), whereas the 2nd anodization duration has less influence on the pore arrangement than the 1st anodization duration. However, longer 1st anodization duration (greater than 2 h) gives little further improvement to the ordering of the pore structure. Taking the ordering of the pore

arrangement and the sample preparation efficiency into account, 1st anodization duration of 2 h was used as the optimal condition in this research.

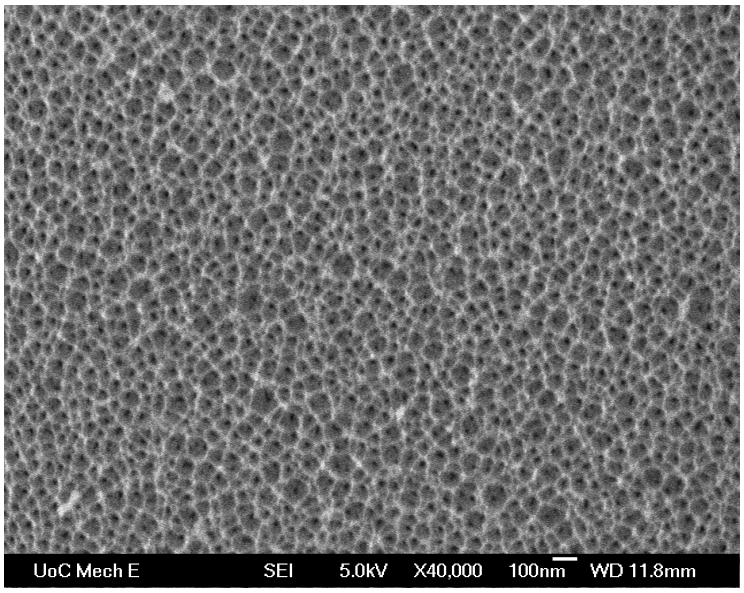

Fig 3.10 FESEM image of top view of sample 9 (1h/1h) after the 2nd anodization.

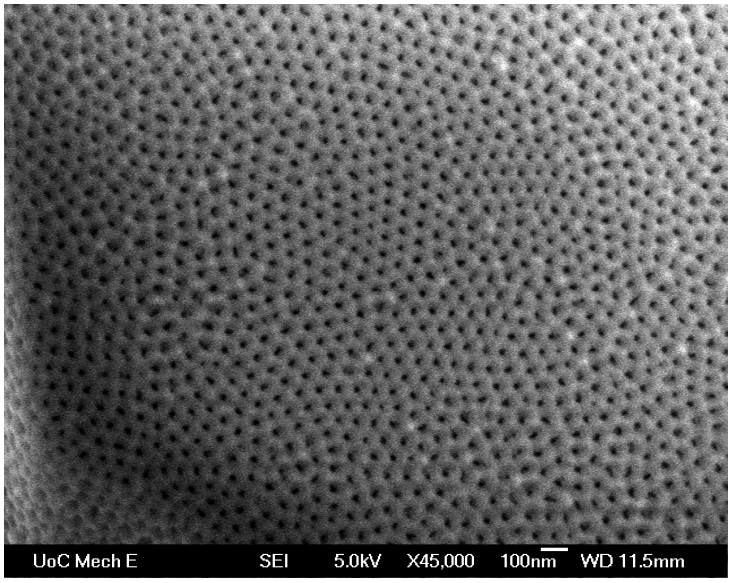

Fig 3.11 FESEM image of top view of sample 10 (2h/1h) after the 2nd anodization.

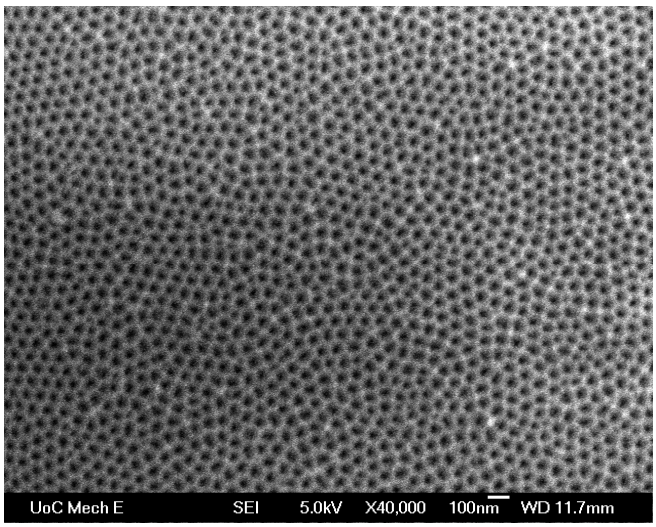

Fig 3.12 FESEM image of top view of sample 11 (4h/30min) after the 2nd anodization.

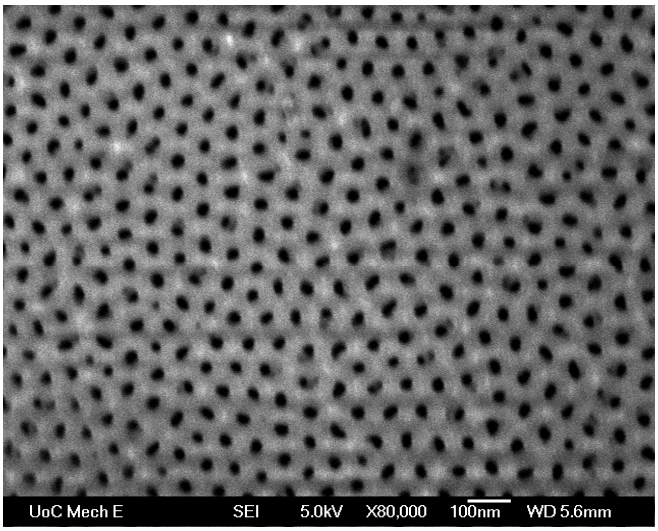

Fig 3.13 FESEM image of top view of sample 12 (4h/1h) after the 2nd anodization.

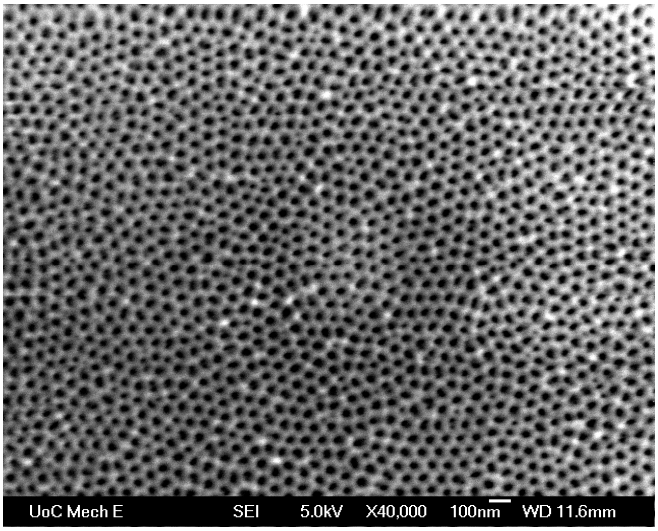

Fig 3.14 FESEM image of top view of sample 13 (4h/2h) after the 2nd anodization.

Anodization duration not only affects the ordering of pore arrangement, but also affects the thickness of the PAA membrane. To study this effect, the following experiments listed in Table 3.6 were carried out. Samples were prepared using a 4 h 1st anodization followed by a 2nd anodization of variable duration. After completion of the 2nd anodization, the thickness of the PAA membrane was measured by FESEM and profilometry.

Table 3.6 Samples prepared for the study of the effect of anodization duration on PAA membrane thickness.

PAA Sample	**Anodizing conditions**	**Anodizing duration (1st/2nd)(h)**
14	30 V 0.4M oxalic acid ~16 °C 1000 rpm	4h/0h
14’		4h/0h
15		4h/30min
15’		4h/30min
16		4h/1h
16’		4h/1h
17		4h/2h
17’		4h/2h

Sample 14 was cut in half. The membrane thickness of one half of the sample 14 (sample 14-1) was measured by a profilometer, and the other half (sample 14-2) was measured by FESEM.

To prepare the sample for thickness measurement using profilometer, sample 14-1 was immersed in a solution containing 0.2 M H_2CrO_4 and 0.8 M H_3PO_4 for 60 min at approximately 65 °C to remove the PAA membrane. Since, the edge of the Al disc was not anodized (because it is not exposed to the electrolyte during anodization), there will be a height difference between the edge and the anodized area after the PAA membrane is removed. The height difference is the membrane thickness, and it can be measured using the profilometer.

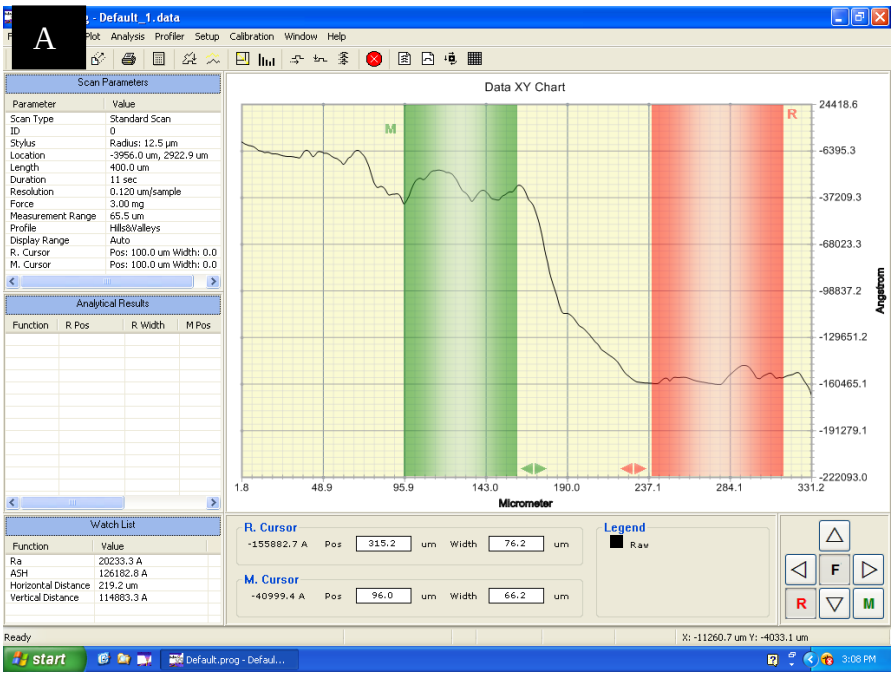

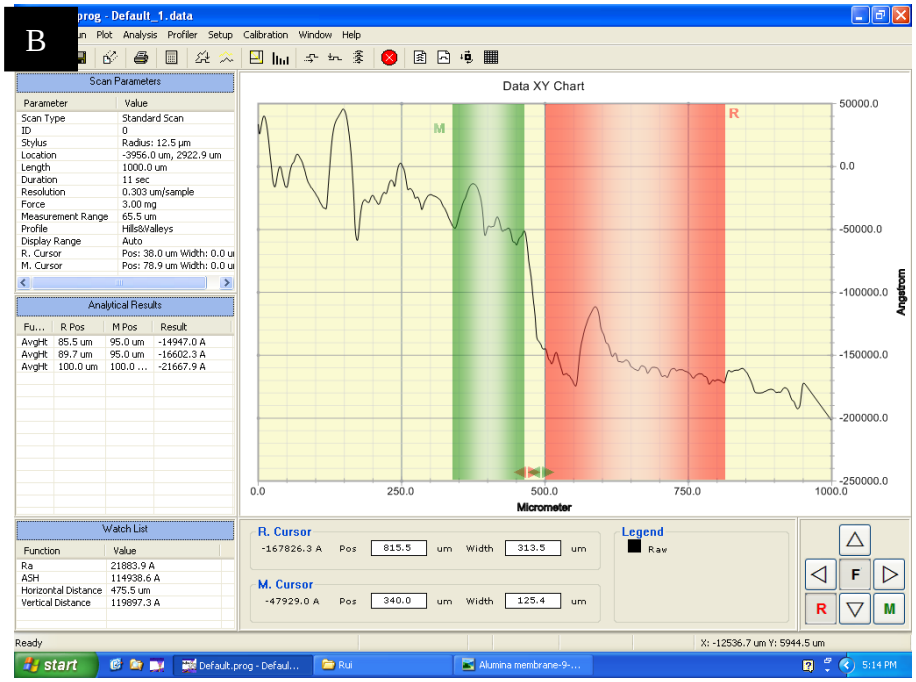

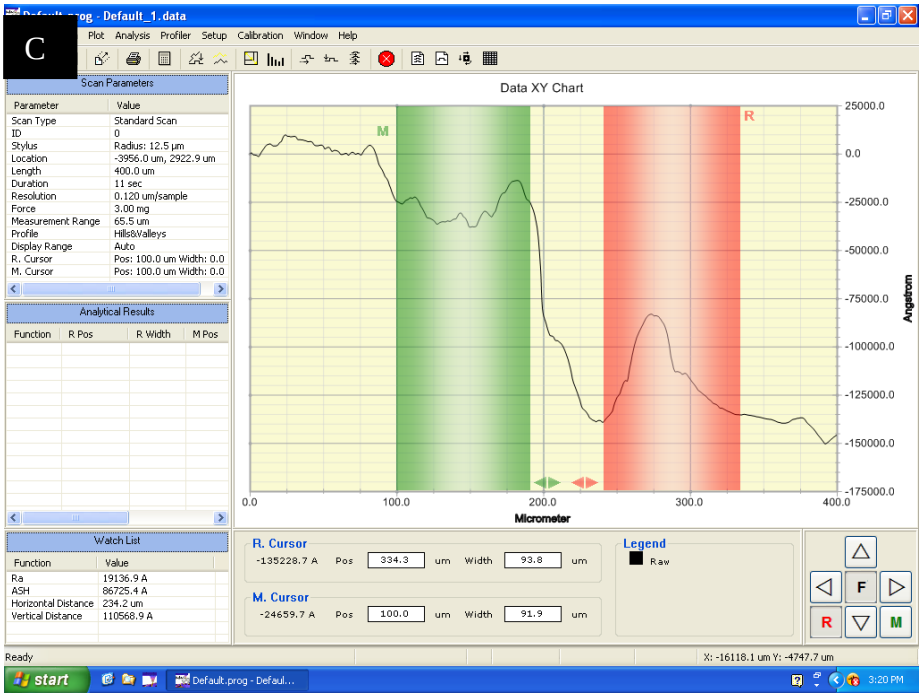

Fig 3.15 Profilometer measurements of sample 14-1 at different starting points (A, B, C).

As shown in Fig 3.15, the profilometer measurement did not provide good information on the PAA membrane thickness due to the roughness of the Al surface. Three different starting points (A, B, C) were randomly selected, and the surface scans showed a very rough surface with the average vertical height between the upper level and the lower level of 11.4 • m, 11.9 • m, and 11.1 • m for A, B and C respectively.

Clearly, the PAA membrane thickness is proportional to the anodization duration. 4-h anodization duration should give the thickest PAA membrane among these samples listed in Table 3.6. It was assumed that for thinner PAA membranes, the roughness of the surface would make it difficult to obtain a reliable profilometer measurement. Therefore, FESEM was then used to measure the PAA membrane thickness.

To measure the membrane thickness using FESEM, a clean cut of a cross-section of the PAA sample is needed. All the sample except for sample 14-1 were partially immersed in a solution containing 0.51 g of $CuCl_2$, 25 mL of DW and 5 mL of HCl (38%) to remove the Al substrate. After approximately 30 min, the Al substrate immersed in the solution was removed from the sample, leaving a transparent PAA membrane. During this detaching process, the unsupported PAA membrane was snapped off the sample, leaving a clean cross-section of PAA membrane on the remaining Al substrate (Al base without exposure to the solution).

FESEM images of their cross-sectional views are shown in Fig 3.16. Summary of the obtained data is presented in Table 3.7

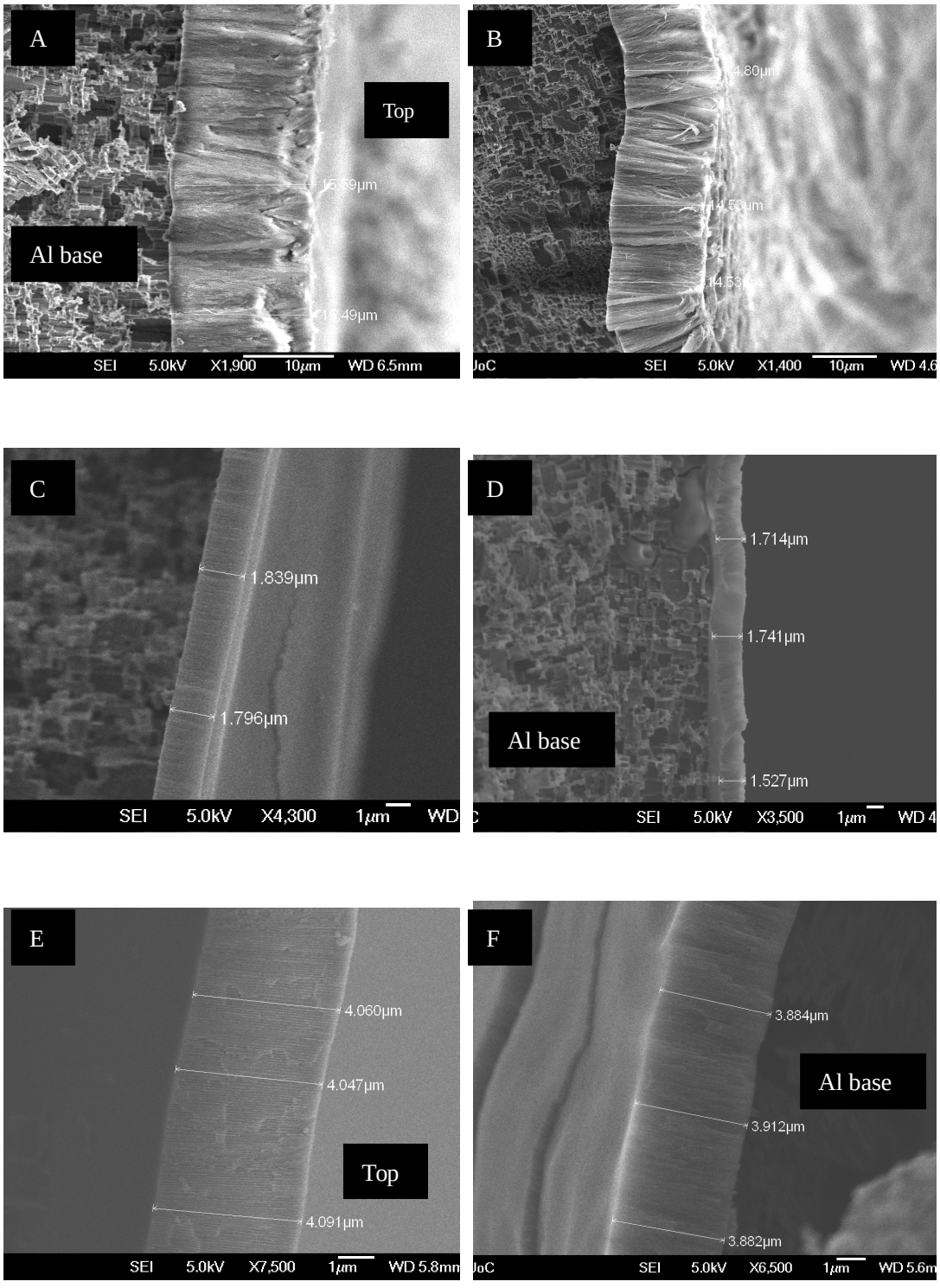

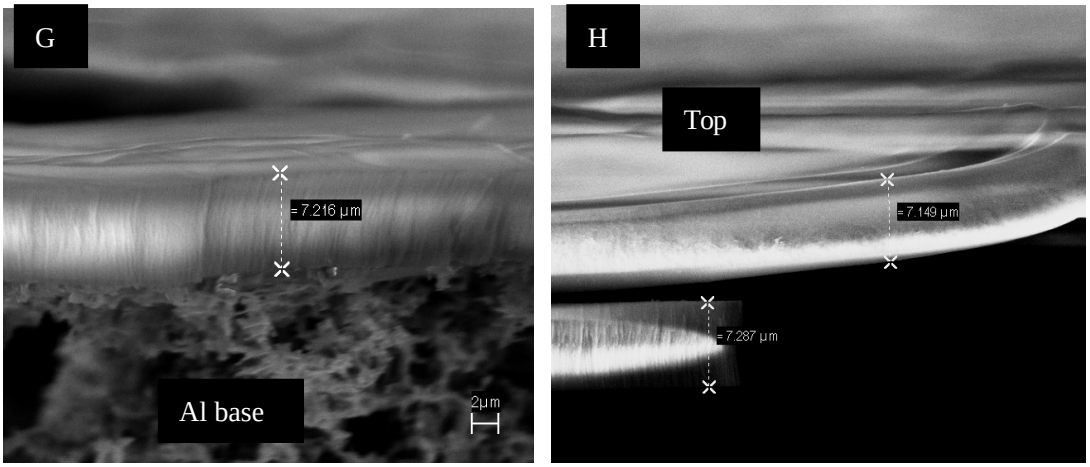

Fig 3.16 FESEM images of cross-section view of (A) sample 14-2, (B) sample 14', (C) sample 15, (D) sample 15', (E) sample 16, (F) sample 16', (G) sample 17 and (H) sample 17'.

Table 3.7 Membrane thickness of the samples measured by FESEM

Sample	**Anodizing Conditions**	**Anodizing duration (1st/2nd)(h)**	**Average PAA membrane thickness (• m)**
14-2	30 V 0.4M oxalic acid ~16 °C 1000 rpm	4h/0h	15.7
14'		4h/0h	14.6
15		4h/30min	1.8
15'		4h/30min	1.6
16		4h/1h	4.0
16'		4h/1h	3.9
17		4h/2h	7.2
17'		4h/2h	7.2

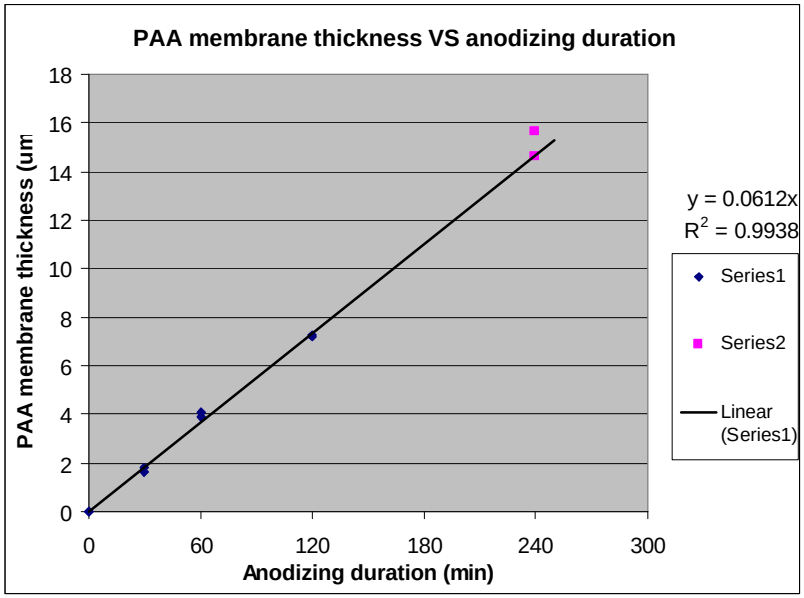

Fig 3.17 The relationship between the anodizing duration and the membrane thickness.

The membrane thickness was measured using the software of the FESEM. Fig 3.17 shows a linear relationship between the anodization duration and the membrane thickness, and the rate of growth under the above processing conditions is 3.7 • m/h. This linear relationship is expected based on the current density *vs* time behaviour shown in Fig 3.5. Fig 3.5 slows that during the 2nd anodization, the current density rapidly reaches steady state (point C') indicating a constant rate of pore growth.

3.3 Conclusions

The pore formation of the PAA membrane was carefully studies, and three ways of preparing ordered PAA templates were examined. The result showed that electropolishing provides Al foil a favourable surface morphology to the anodization. However, the electrolyte used for electropolishing was very corrosive to the mounting screws and the O-rings of the teflon anode. Therefore, two-step anodization on non-electropolished Al foils was used.

Examination of ordering of the pore arrangement via controlling the anodizing duration indicated that 2 h 1^{st} anodization was the optimal condition in terms of the ordering of pores and time efficiency, and the 2^{nd} anodization duration had less influence on the pore arrangement than the 1^{st} anodization duration. Moreover, the pore diameter was found to increase with an increasing anodizing temperature.

The study of membrane thickness by varying the anodizing duration showed a linear relationship, and an average membrane growth rate of 3.7 • m/h during the 2^{nd} anodization under the given conditions was obtained. This will allow us to select correct 2^{nd} anodization times needed to obtain membranes of particular thickness in future work.

References

[1] A. Huczko, *Applied Physics a-Materials Science & Processing* **2000**, *70*, 365-376.
[2] Y. Z. Piao and H. Kim, *Journal of Nanoscience and Nanotechnology* **2009**, *9*, 2215-2233.
[3] a) J. Li, C. Papadopoulos, J. M. Xu and M. Moskovits, *Applied Physics Letters* **1999**, *75*, 367-369; b) J. S. Suh and J. S. Lee, *Applied Physics Letters* **1999**, *75*, 2047-2049.
[4] a) K. Nielsch, F. Muller, A. P. Li and U. Gosele, *Advanced Materials* **2000**, *12*, 582-586; b) Z. F. Zhou, Y. C. Zhou, Y. Pan and X. G. Wang, *Materials Letters* **2008**, *62*, 3419-3421; c) Y. Piao, H. Lim, J. Y. Chang, W. Y. Lee and H. Kim, *Electrochimica Acta* **2005**, *50*, 2997-3013.
[5] D. D. Li, C. H. Jiang, X. Ren, M. C. Long and J. H. Jiang, *Materials Letters* **2008**, *62*, 3228-3231.
[6] O. Jessensky, F. Muller and U. Gosele, *Applied Physics Letters* **1998**, *72*, 1173-1175.
[7] Z. X. Su, G. Hahner and W. Z. Zhou, *Journal of Materials Chemistry* **2008**, *18*, 5787-5795.
[8] J. H. Yuan, F. Y. He, D. C. Sun and X. H. Xia, *Chemistry of Materials* **2004**, *16*, 1841-1844.
[9] F. Y. Li, L. Zhang and R. M. Metzger, *Chemistry of Materials* **1998**, *10*, 2470-2480.
[10] H. Masuda and K. Fukuda, *Science* **1995**, *268*, 1466-1468.
[11] Y. C. Zhao, M. Chen, Y. N. Zhang, T. Xu and W. M. Liu, *Materials Letters* **2005**, *59*, 40-43.
[12] A. Belwalkar, E. Grasing, W. Van Geertruyden, Z. Huang and W. Z. Misiolek, *Journal of Membrane Science* **2008**, *319*, 192-198.
[13] H. Asoh, K. Nishio, M. Nakao, T. Tamamura and H. Masuda, *Journal of the Electrochemical Society* **2001**, *148*, B152-B156.
[14] K. Nielsch, J. Choi, K. Schwirn, R. B. Wehrspohn and U. Gosele, *Nano Letters* **2002**, *2*, 677-680.
[15] M. T. Wu, I. C. Leu and M. H. Hon, *Journal of Vacuum Science & Technology B* **2002**, *20*, 776-782.
[16] L. B. Kong, Y. Huang, Y. Guo and H. L. Li, *Materials Letters* **2005**, *59*, 1656-1659.
[17] A. Rauf, M. Mehmood, M. A. Rasheed and M. Aslam, *Journal of Solid State Electrochemistry* **2009**, *13*, 321-332.
[18] D. Ma, S. Li and C. Liang, *Corrosion Science* **2009**, *In Press, Corrected Proof*.
[19] J. M. Montero-Moreno, M. Sarret and C. Muller, *Surface & Coatings Technology* **2007**, *201*, 6352-6357.

[20] Report on Self-Ordered Porous Alumina Template Technology. [Online]www.wiki.bath.ac.uk.

Chapter 4: Synthesis of CNTs using Thermal CVD

4.1 Introduction

Porous anodic alumina has been widely used as a template for nanofabrication. In this research, PAA templates were used for growing carbon nanotubes using thermal CVD. There are three steps involved in this synthesis process: PAA template preparation, electrodeposition of metal catalyst and CNT growth[1]. The PAA template preparation has discussed in Chapter 3. In this chapter, electrodeposition and CNT growth will be discussed.

Metal catalyst can be electrochemically deposited at the bottom of the pores of PAA templates by applying either direct current (DC) or alternating current (AC)[2],[3]. The catalyst-loaded PAA templates are then used for growing CNTs in a thermal CVD system. Li *et al.*[1] and Suh *et al.*[4] fabricated well-aligned arrays of CNTs from PAA templates embedded with Co catalyst by pyrolyzing C_2H_2 at 650 ºC-700 ºC. Iwasaki *et al.*[5] and Jeong *et al.*[6] have reported that CNTs are not confined in the pores of PAA templates and can overgrow from the pores during the pyrolysis of C_2H_2 with added H_2. They have suggested that overgrowth of the CNTs from the pores is due to the presence of the H_2 flow during the pyrolysis, and this is because H_2 prevents deactivation of the metal catalyst caused by deposition of amorphous carbon on the

active sites of the catalyst as the reaction proceeds. Many studies have showed that the CNT growth on PAA templates varies with different CVD conditions[1],[7],[8],[9],[10].

This chapter discusses results of cobalt electrodeposition and growth of CNTs from Co-loaded PAA templates and on Si chips using thermal CVD.

4.2 Results and Discussion

4.2.1 Carbon Nanotube Growth on Si Chips

Prior to the study of the templated synthesis of carbon nanotubes, the following experiments were carried out. The purpose was to become familiar with use of the thermal CVD system for CNT preparations.

Three clean Si chips were prepared as described in Chapter 2 and the experimental conditions are shown in Table 4.1. SEM images of the prepared CNTs are shown in Fig 4.1

Table 4.1 Experimental conditions used for growing CNTs on Si chips

Si chip	Metal deposition	CNT growth
Sample-1	10 nm of Al followed by 10 nm of Fe was deposited on the Si chip by an Edwards 3000 e-beam evaporator.	The samples were reduced at 750 ºC for 30 min with gas flows of Ar: 1200 sccm and H_2: 800 sccm. Then, CNTs were grown at 750 ºC for 15 min with gas flows of Ar: 1000 sccm, H_2: 800 sccm, C_2H_4: 400 sccm and Ar/H_2O: 50 sccm.
Sample-2	~1 mL of 0.01 M of a catalyst solution containing $Fe(NO_3)_3$and $Al(NO_3)_3$ was applied to the Si surface and then dried in air at ~60 °C	
Sample-3	~1 mL of 0.02 M of the catalyst solution was applied to the Si surface and then dried in air at ~60 °C	

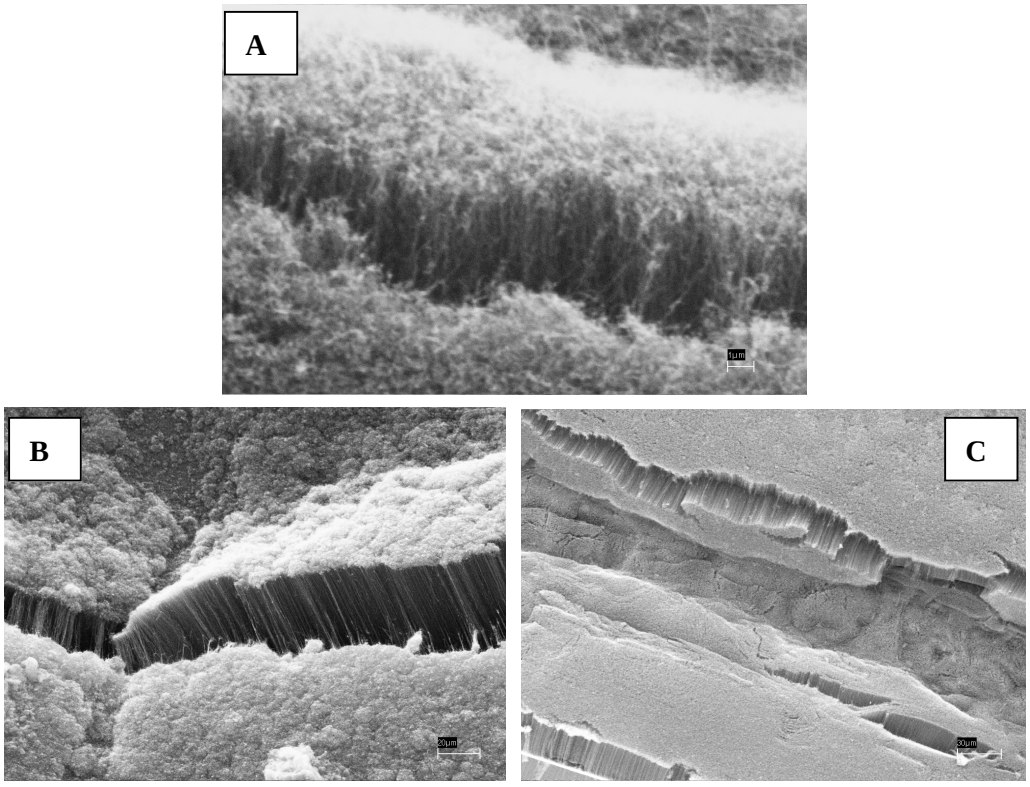

Fig 4.1 SEM images of (A) sample-1, (B) sample-2 and (C) sample-3 after CNT growth.

Carbon nanotubes were grown in dense carpets for all three samples as shown in Fig 4.1. The vertical alignment of the CNTs results from steric crowding and van der Waals interactions between each CNT[11],[12]. Clearly, as the CNT density decreases, these factors will have less influence on the alignment. Liu, a post-doctor who worked for Prof. Alison Downard, has reported that the minimum accessible diameter of VACNT bundles synthesized directly by thermal CVD is confined to 2 • m[13].

Use of PAA templates provides an alternative approach towards vertical alignment of CNTs so that smaller bundles of VACNTs or even individual VACNTs can be prepared. The following sections will focus on the PAA template-based synthesis of CNTs using thermal CVD.

4.2.2 Electrodeposition of Cobalt

The anodization of Al leads to an insulating barrier layer at the bottom of the pores that prevents direct contact between the conducting Al cathode and the electrodeposition electrolyte. Two different methods have been developed for uniform and complete filling of the pores by electrodeposition.

In the first method, the PAA membrane is detached from the Al substrate. Subsequently, the barrier layer is removed from the membrane by a chemical etching

process. Then, a metallic contact is sputtered on one side of the free-standing membrane and the membrane is used as a cathode for electrodeposition. This method is applicable for free-standing membranes that are thick enough (>20 • m) and mechanically stable enough to be handled[2],[3].

In the second method, AC electrodeposition is used after a barrier layer thinning treatment. Here, the PAA membrane stays on the supporting Al substrate, and the barrier layer can be thinned either by gradually dropping the anodizing voltage at the end of the 2nd anodization, or by chemical etching.

Although the barrier layer blocks direct current with a very high resistance, under alternating current, the aluminum oxide conducts preferentially in the cathodic direction. This rectifying property of the barrier layer allows the reduction of ions in the pores during cathodic half-cycles, without allowing re-oxidation during the anodic half-cycles[14]. The barrier layer thinning treatment results in a considerable decrease in the potential barrier for the electrons to tunnel through the barrier layer during electrodeposition.

In this research, all PAA templates prepared for electrodeposition were less than 10 • m thick. Moreover, the process for detaching the PAA membrane from the Al base could be time consuming since the original Al foil was 0.5 mm thick. Therefore, the AC electrodeposition method described above was used to deposit Co at the bottom of

the pores of PAA templates for CNT growth.

4.2.2.1 Barrier Layer Thinning

Table 4.2 shows the barrier layer thinning processes used for three PAA templates. After each thinning process, the samples were examined using FESEM. The purpose of this experiment was to examine the thinning effect of each process on the barrier layer.

Table 4.2 Samples prepared to examine the barrier layer thinning processes

Sample	**Barrier layer thinning process**
PAA-1	A gradual voltage drop at the end of the 2nd anodization
PAA-2	Chemical etching
PAA-3	A combination of the above two processes

Note: anodization conditions: 30 V, 0.4 M $H_2C_2O_4$, 16 ºC, 1000 rpm, 2 h 1st anodization and 1 h 2nd anodization.

PAA-1, 2 and 3 were prepared under identical conditions. For PAA-1, a gradual voltage drop from 30 V to 10 V at a rate of ~1 V/min was applied at the end of the 2nd anodization. For PAA-2, the sample was immersed in 0.1 M H_3PO_4 at approximately 30 °C for 1 h. For PAA-3, the same voltage drop process as for PAA-1 was used and followed by the same chemical etching process as for PAA-2.

Since the pore diameter is proportional to the anodizing voltage, a decrease in the anodizing voltage will lead to a series of small holes at the bottom of the pores resulting in a decrease in the barrier layer thickness[15]. Many studies[3],[15],[16],[17] have found that the barrier layer thickness is dependent upon the anodization voltage with a relationship of ~1 nm/V^{-1}. Based on this relationship, the thickness of the barrier layer of PAA-1, 2 and 3 should be around 30 nm. Unfortunately, it was very difficult to obtain a cross-section view of a PAA membrane that was clear enough to measure such a thin layer. Fig 4.2B was one of the best FESEM images of cross-section view of a PAA membrane.

FESEM images of the three PAA samples after the barrier layer thinning treatment are shown in Figs 4.2-4.4. Sample preparation for imagining the cross-section of PAA-1 is described in Chapter 2.

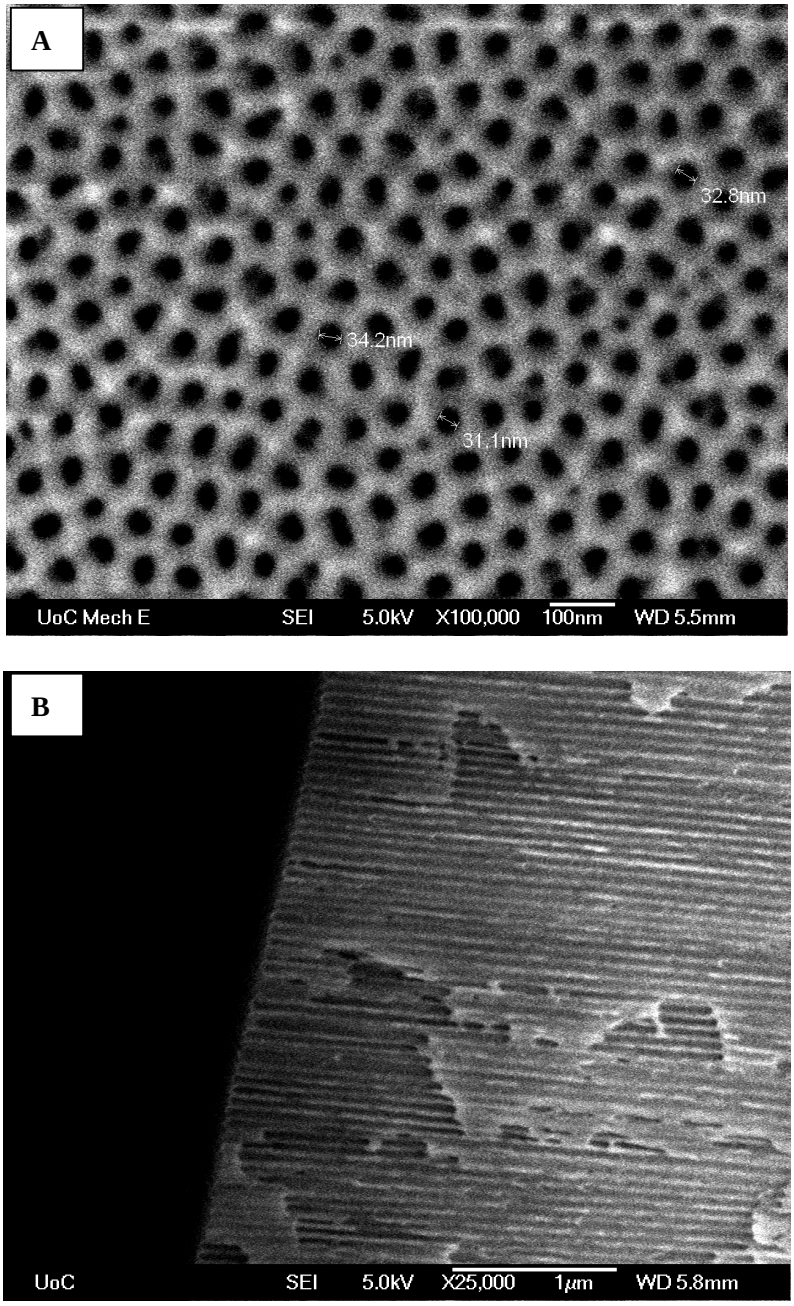

Fig 4.2 FESEM images of (A) top view of PAA-1 and (B) cross-section view of PAA-1 after the voltage drop process.

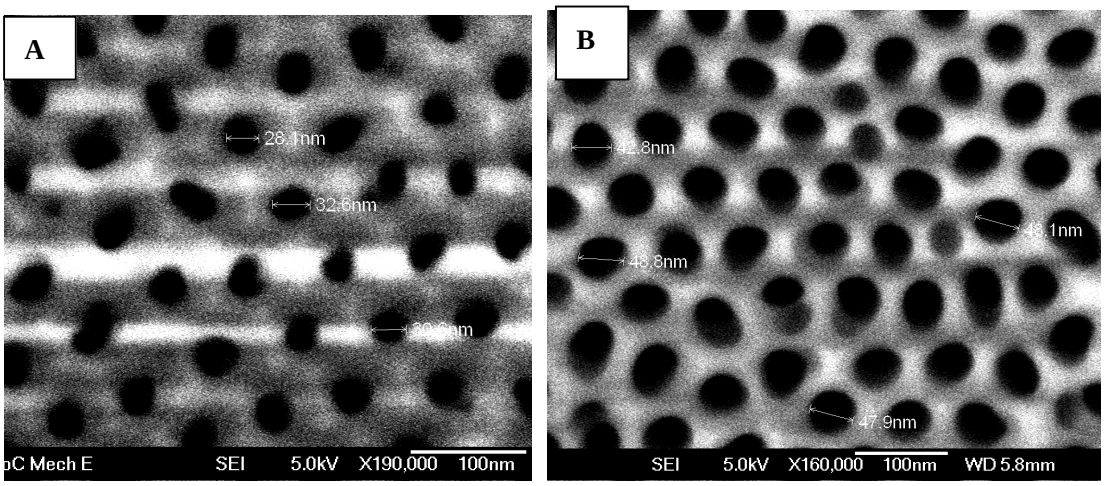

Fig 4.3 FESEM images of top view of PAA-2 (A) before chemical etching and (B) after chemical etching.

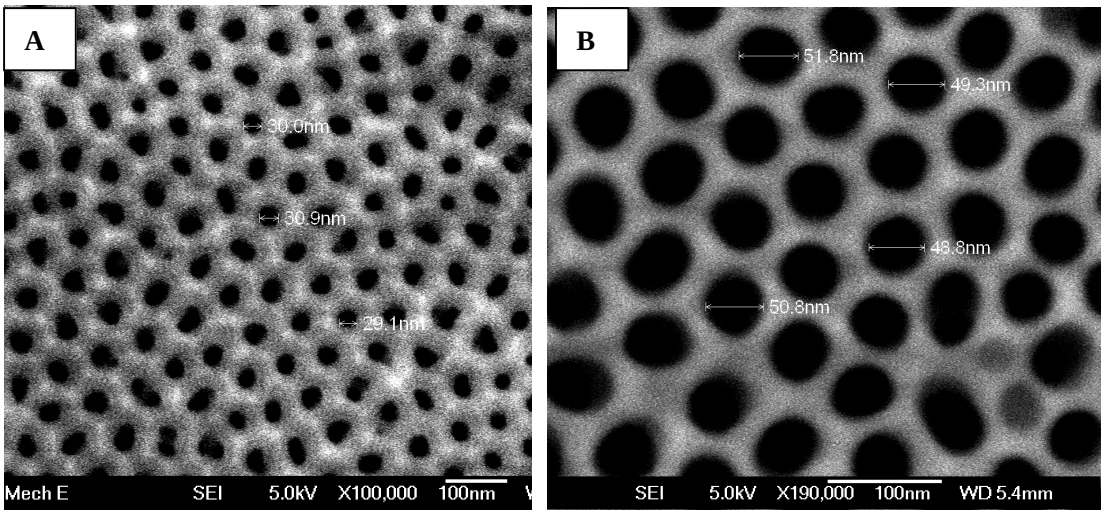

Fig 4.4 FESEM images of top view of PAA-3 (A) before chemical etching and (B) after chemical etching.

The chemical etching process enlarges the pores as well as thins the barrier layer. The pore widening effect was observed using FESEM as shown in Fig 4.3 and Fig 4.4. An average pore diameter of 30 nm (PAA-2 and PAA-3) was widened to ~48 nm for PAA-2 and ~50 nm for PAA-3. However, it was unable to observe any thinning effect on the barrier layer due to a limitation of the ability to obtain a clear cross section

image using FESEM.

Although the barrier layer thinning effect was not observed directly under the microscope, there was another way to examine these thinning processes. AC electrodeposition of Co catalyst at the bottom of the pores was used as an indirect measurement of this effect.

Table 4.3 Examination of the barrier layer thinning processes by AC electrodeposition

Sample	**Barrier layer thinning process**	**Deposition conditions**
PAA-1	A gradual voltage drop at the end of the 2nd anodization	10 V_{peak}, 100 Hz square waveform with reductive/oxidative (5 ms/5 ms) pulse polarity, for 30 s
PAA-2	Chemical etching	
PAA-3	A combination of the above two processes	

The previous samples PAA-1, 2 and 3 (after barrier layer thinning) were immersed in a solution containing 240 g/L $CoSO_4 \cdot 7H_2O$ and 40 g/L H_3BO_3 for 15 min to allow diffusion of Co^{2+} ions into the pores before electrodeposition. The electrodeposition conditions were the same for all the samples as shown in Table 4.3. During electrodeposition, formation of H_2 bubbles on the membrane surface was observed. This may be due to the depletion of the Co^{2+} ions concentration at the deposition interface[3]. A color change on the deposition surface was also observed during the

electrodeposition. For PAA-1, a silvery surface was turned into a weak brownish color, but the color was not smoothly spread. For PAA-2, a darker brown color was found on the surface and the color was well spread around the center of the surface; a mix of blue and brown color was found around the edge of the deposition area. For PAA-3, the surface had a uniform blue color after the electrodeposition.

The color change observed after electrodeposition is believed to be due to the deposition of Co in the pores. However, the origin of the different colors (blue or brown) is unknown. Co is expected to be readily oxidized and it is possible that the colors are due to cobalt oxide. The weak color of PAA-1 is attributed to a smaller amount of deposited Co than for PAA-2 and PAA-3. Based on the superior uniformity of the color for PAA-3, the two-step barrier layer thinning method is considered the most effective thinning treatment for AC electrodeposition.

Fig 4.5 shows a cross-section view of the membrane of PAA-3 after the electrodeposition. It is assumed that the bright columns at the bottom of the pore are Co deposits.

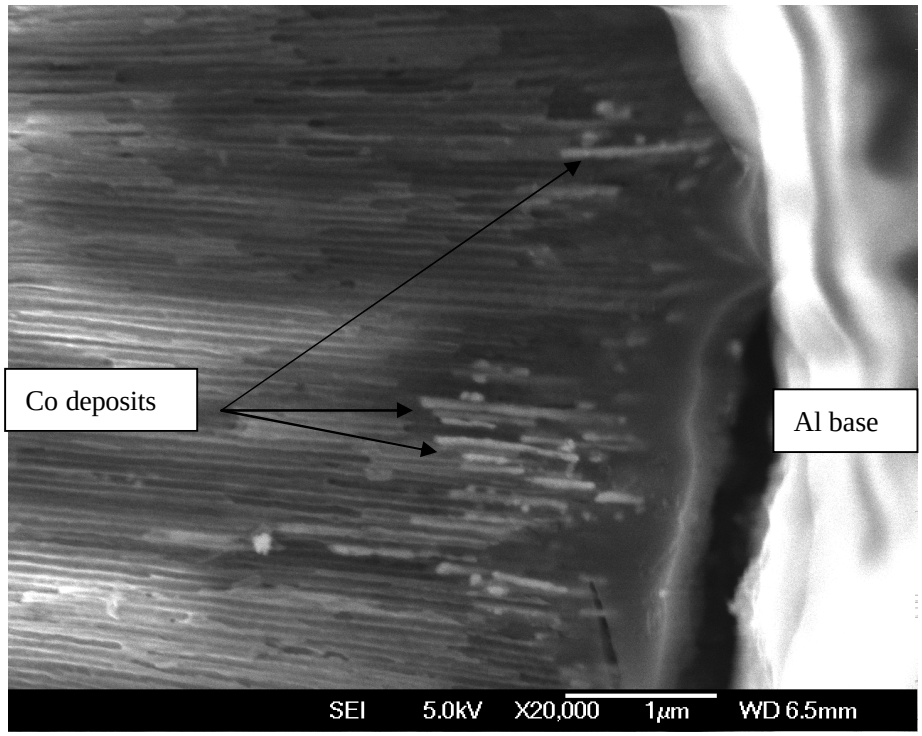

Fig 4.5 FESEM image of cross-section view of PAA-3 after electrodeposition of Co.

4.2.2.2 Electrodeposition Conditions

In general, AC electrodeposition through the barrier layer is a complicated process. Many studies have showed that there is a variation in the quality of pore-filling as a function of deposition conditions, including electrolyte concentration, composition and temperature, and deposition voltage, frequency, waveform, polarity and deposition duration[2],[14],[18]. This is not surprising because the chemical and structural nature of the barrier layer is complex, particularly after barrier layer thinning. In addition, it is possible that the structure of the barrier layer will be modified during AC electrodeposition.

In this research, deposition conditions as shown in Table 4.4 were chosen based on the study of Nielsch *et al.*[3], Gerein *et al.*[14] and Li *et al.*[19]. However, the available electrodeposition setup as shown in Fig 2.5 in Chapter 2 limited chooses of deposition voltage, waveform and temperature.

Table 4.4 Electrodeposition conditions

Electrolyte	A aqueous solution containing 240 g/L $CoSO_4 \cdot 7H_2O$ and 40 g/L H_3BO_3
Deposition Voltage	10 V_{peak} (Max)
Deposition Frequence	100 Hz
Deposition Waveform	Square waveform
Deposition Duration	Variable
Deposition Temperature	Room temperature
Polarity	Reductive/Oxidative (5 ms/5 ms)

The following experiment shown in Table 4.5 was used to establish a suitable range of electrodeposition time for subsequent experiments. Prior to electrodeposition, the PAA samples were soaked in the electrolyte overnight on an orbital shaker. The purpose of this immersion step was to allow enough time for diffusion of Co^{2+} ions into the pores.

Table 4.5 Electrodeposition of Co under the same conditions as shown in Table 4.4 for different durations

Sample	**Anodization conditions**	**Barrier layer thinning**	**Deposition duration**
PAA-4	30 V, 0.4 M oxalic acid, 16 ± 1 ºC, 1000 rpm, 2 h/1 h	A gradual voltage drop from 30 V to 10 V at a rate of ~1V/min at the end of the 2nd anodization followed by a chemical etching process in 0.1 M H_3PO_4 at ~ 30 °C for 1 h	10 s
PAA-5			30 s
PAA-6			3 min
PAA-7			9 min
PAA-8			15 min
PAA-9			20 min
PAA-10			30 min

For all samples, a color change and formation of H_2 bubbles were observed as soon as the voltage was applied. After the electrodeposition, it was found that PAA-4 had the weakest color, PAA-5, 6, 7 and 8 had a similar color, and PAA-9 and 10 had a similar color, but were darker than other samples. All samples were then examined using FESEM.

FESEM images of top view of PAA-4 to 8 showed only normal PAA membrane surfaces. This means that the pores are not completely filled under the given conditions. FESEM image of PAA-9 showed a very low extent of Co deposition on the membrane surface. These FESEM images are not shown as they provide little information; however the FESEM images of PAA-10 are shown in Fig 4.6.

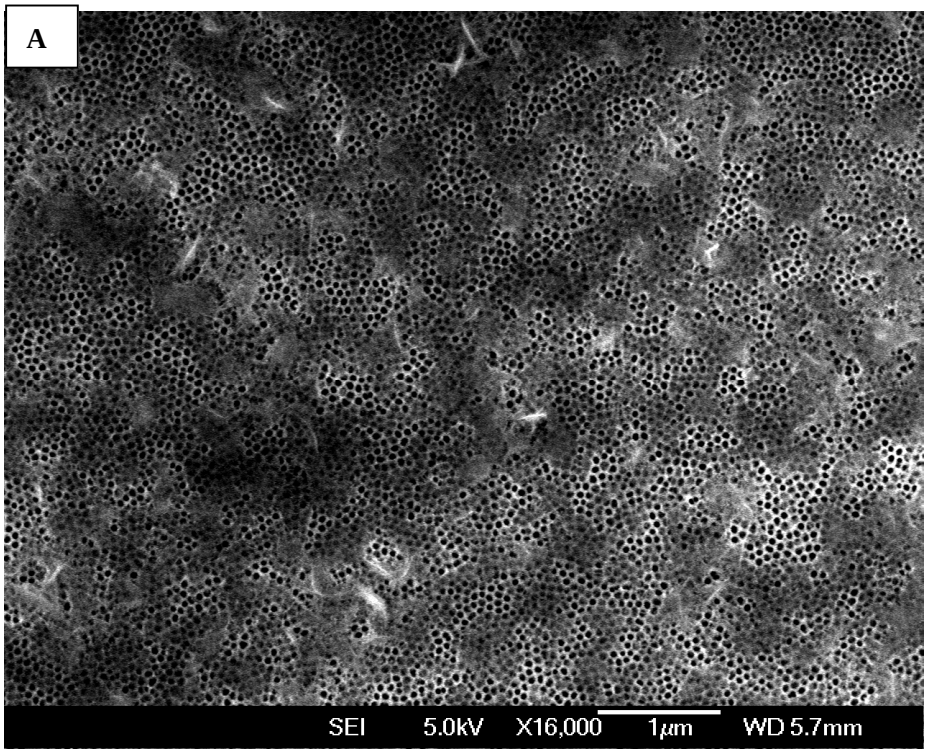
A
SEI 5.0kV X16,000 1μm WD 5.7mm

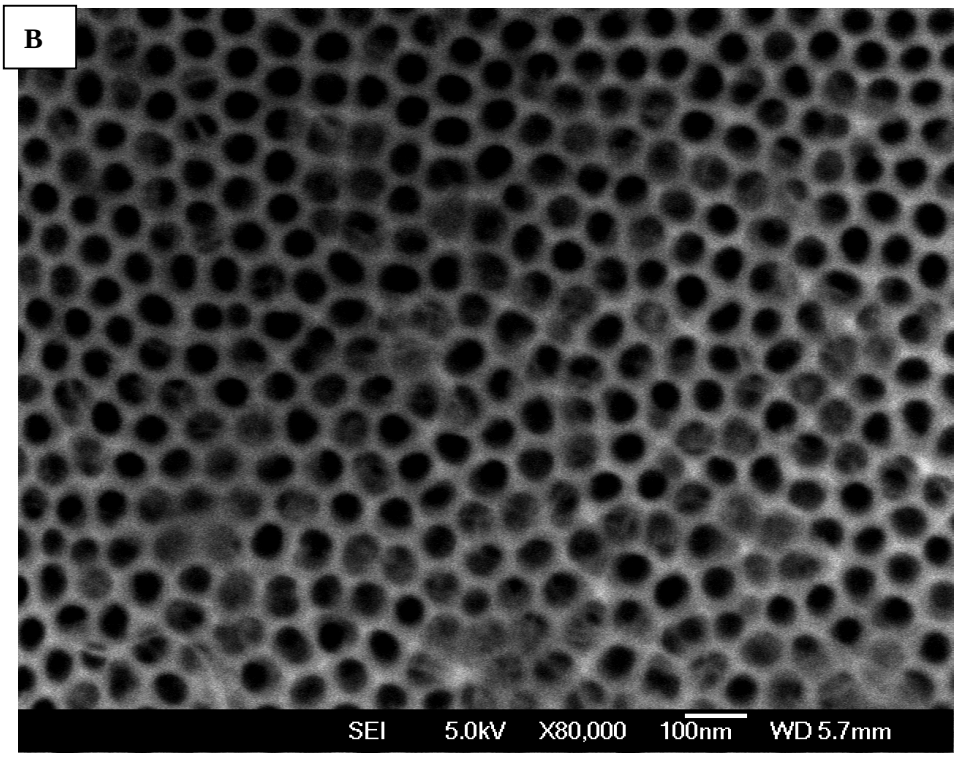
B
SEI 5.0kV X80,000 100nm WD 5.7mm

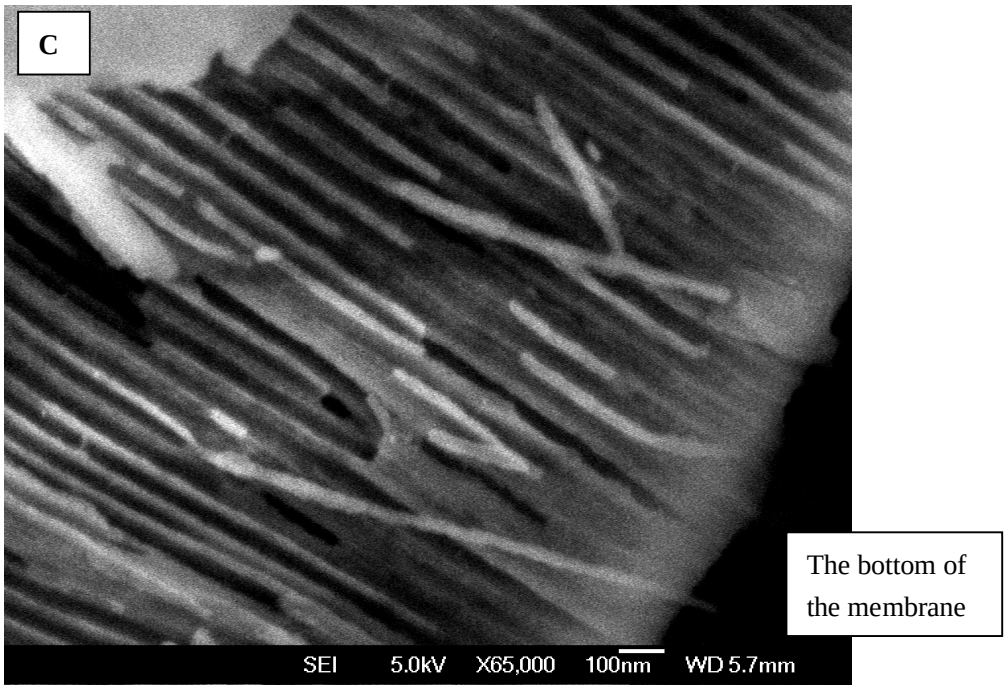

Fig 4.6 FESEM images of PAA-10 after electrodeposition. (A) Top view at a low magnification, (B) top view at a higher magnification and (C) a cross-section view showing Co deposits (bright columns).

Fig 4.6A shows that the PAA membrane surface is partially covered by Co deposits, and many pores are filled by Co as shown in Fig 4.5B. Fig 4.5C shows Co nanowires (bright columns) grown in the pores. This confirms that Co is deposited in the pores. However, it is also shows that a long deposition time will lead to unwanted deposition of Co on the PAA membrane surface.

Because the color change for PAA-4 after 10 s electrodeposition was very weak, it was assumed that only a small amount of Co was deposited. On the other hand, the similar color of PAA-9 and 10 suggests that electrodeposition time longer than 15 min are unsuitable as too much Co is deposited. Therefore, further experiments used

electrodepostion time ranging from 30 s to 10 min under the given conditions.

4.2.3 Synthesis of CNTs using Co-loaded PAA Templates

After electrodeposition of Co at the bottom of the pores, the Co-loaded PAA templates were then used to grow CNTs using thermal CVD. CNTs were successfully grown from PAA-4 to 10 with a variation in the quality of CNT in terms of CNT density, length. In order to study effects of different conditions on CNT growth, the following experiments were carried out.

- *Experiment Set 1*

In set 1, a PAA template was cut into 4 pieces, and each piece was used for an individual experiment with specified conditions. The experimental conditions for anodization, electrodeposition and CNT growth are shown in Table 4.6.

Table 4.6 Experimental conditions for the preparation of PAA, deposition of Co and growth of CNTs (Set 1)

Preparation of PAA	PAA-11 (30 V, 0.4 M oxalic acid, 16 ±1 ºC, 1000 rpm, 2 h/1 h A gradual voltage drop from 30 V to 10 V at a rate of ~1 V/min, then chemical etching in 0.1M phosphoric acid at ~ 30 ºC for 1 h.) PAA-11 was cut into 4 pieces: PAA-11-1, PAA-11-2, PAA-11-3 and PAA-11-4
Electrolytes	1) A solution of 40 g/L boric acid (blank) 2) A solution containing 240 g/L of $CoSO_4$-$7H_2O$ and 40 g/L boric acid (pH ~ 4) PAA-11-2 and PAA-11-3 were soaked in the Co salt solution overnight on an orbital shaker.
Electrodeposition conditions	10 V_{peak}, 100 Hz square waveform with reductive/oxidative (5 ms/5 ms) pulse polarity i) PAA-11-1: Electrodeposition using the electrolyte 1 under the above conditions for 5 min. ii) PAA-11-2: Electrodeposition using the electrolyte 2 under the above conditions for 30 s. iii) PAA-11-3: Electrodeposition using the electrolyte 2 under the above conditions for 150 s. iv) PAA-11-4: No electrodeposition. Drop coating of ~2 mL of the electrolyte 2 on the surface. All samples except for PAA-11-4 were rinsed with DW and then immersed in DW on an orbital shaker overnight before carrying out the CNT growth step.
CNT growth conditions	The samples were reduced at 500 ºC for 1 h with gas flows of Ar: 1000 sccm and H_2: 800 sccm. Then, CNTs were grown at 600 ºC for 10 min with gas flows of Ar: 1000 sccm, H_2: < 100 sccm and C_2H_4: 400 sccm

PAA-11-1 was prepared as a sample blank. “Electrodeposition” was carried out in the absence of the cobalt salt. There was no color change, i.e. no visible reactions, during the electrodeposition process, as expected in the absence of the metal salt. For PAA-11-2 and PAA-11-3, a color change was observed as soon as the electrodeposition voltage was applied, along with generation of H_2 bubbles. After electrodeposition, the original silvery color of the PAA was turned into a bluish color. For PAA-11-4, approximately 2 mL of the Co salt solution was applied to the membrane surface leaving a very weak reddish color on the surface. After CNT growth, a black layer was seen on the Co-loaded area of PAA-11-2, PAA-11-3 and PAA-11-4. No visible changes were seen on the areas of these samples not exposed to the Co salt solution, nor on PAA-11-1.

FESEM images of PAA-11 samples are shown in Figs 4.7-4.10.

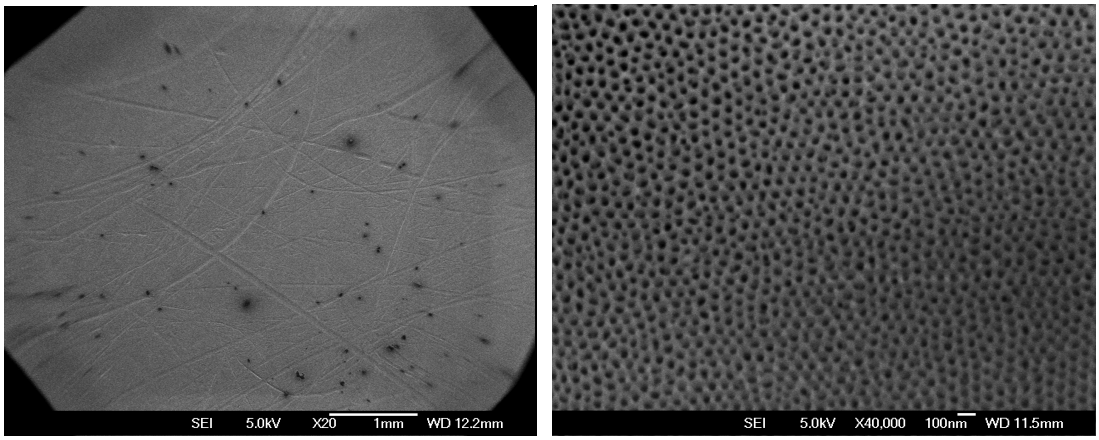

Fig 4.7 FESEM images of top view of PAA-11-1. (Left) An overview of the sample surface. (Right) A closer look at the surface.

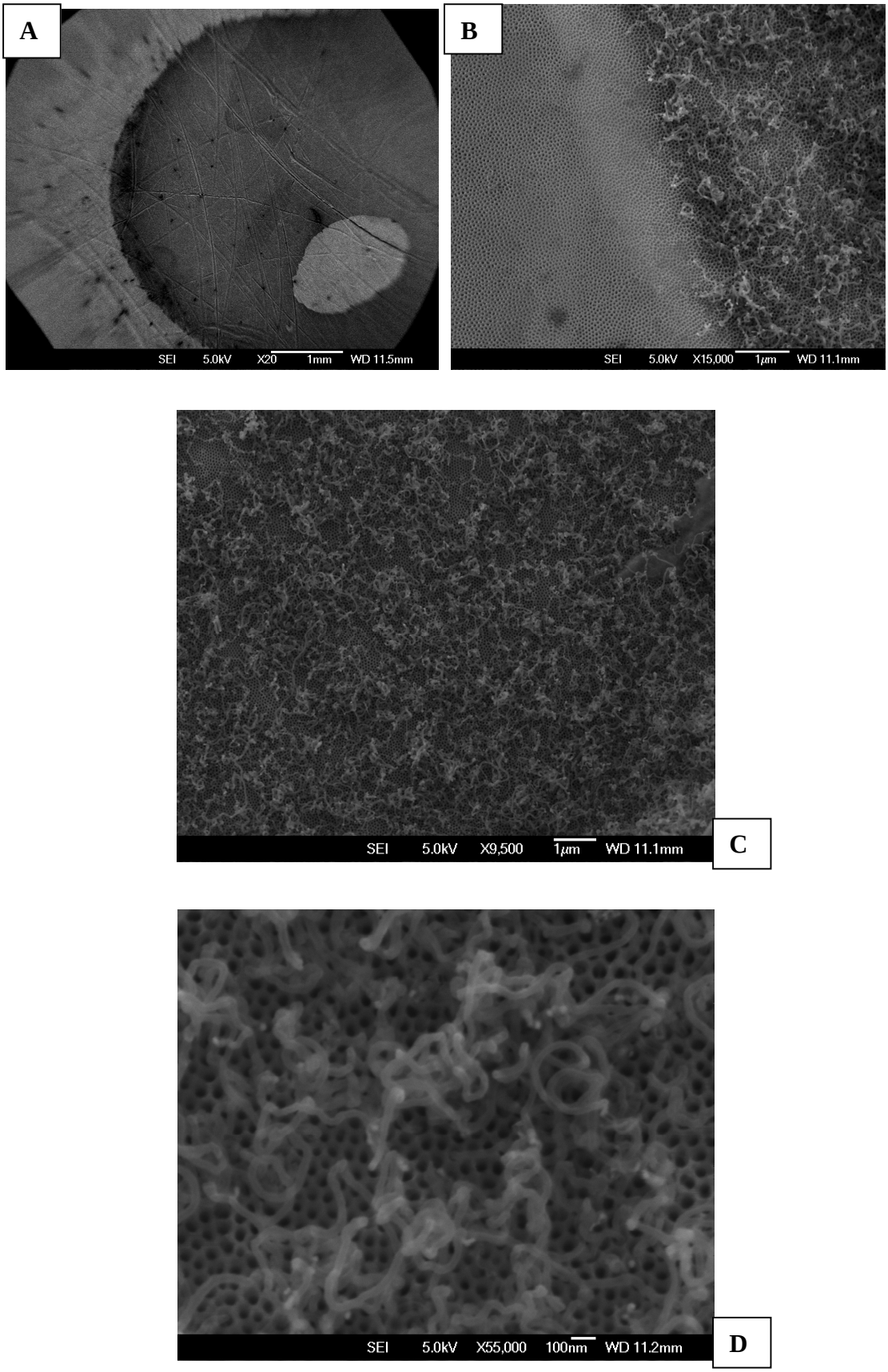

Fig 4.8 FESEM images of top view of PAA-11-2. (A) An overview of the Co-loaded area, (B) the edge of the Co-loaded area, (C) the middle part of the area, (D) A closer look at the middle area.

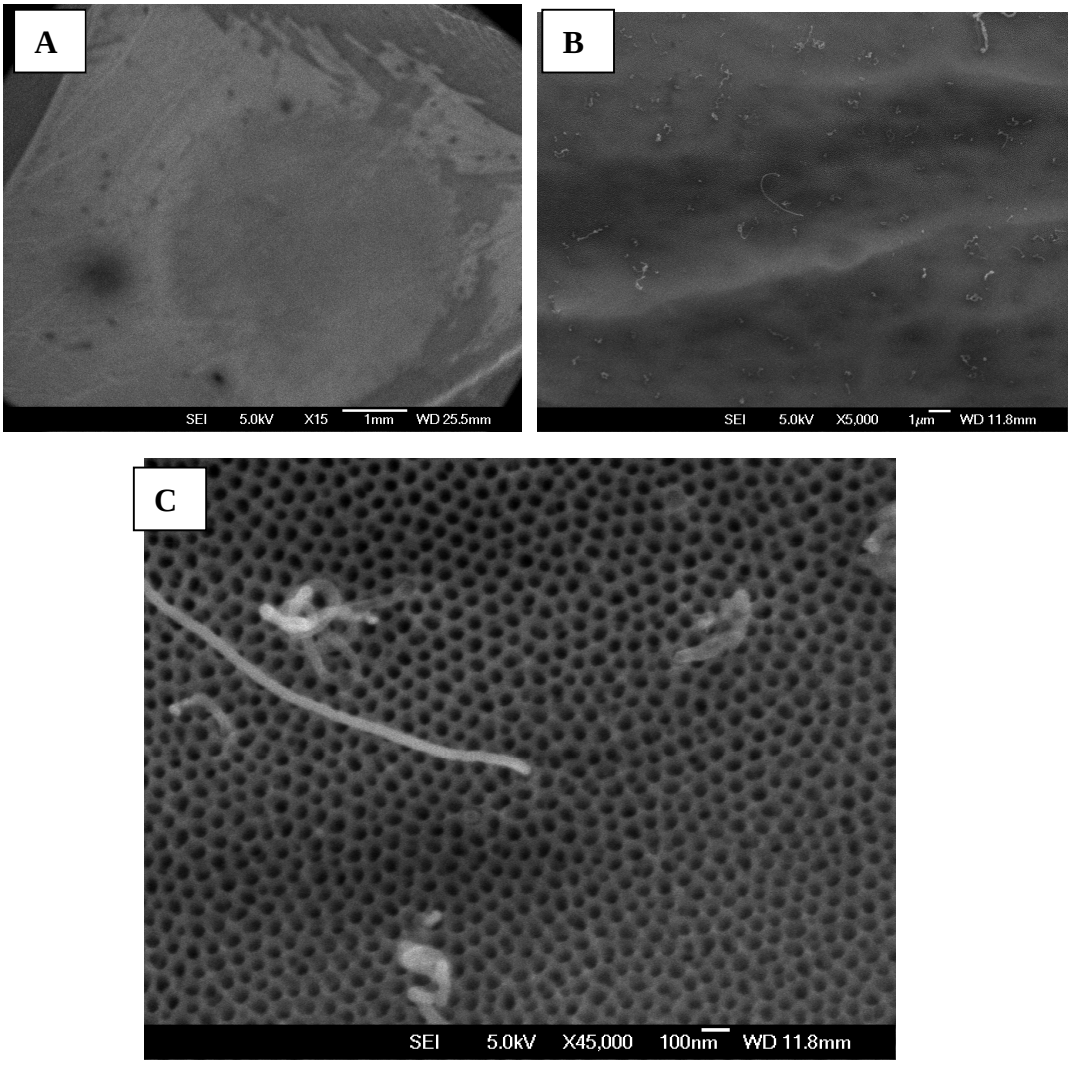

Fig 4.9 FESEM images of top view of PAA-11-3. (A) An overview of the Co-loaded area., (B) the Co-loaded area. (C) A close look at the area.

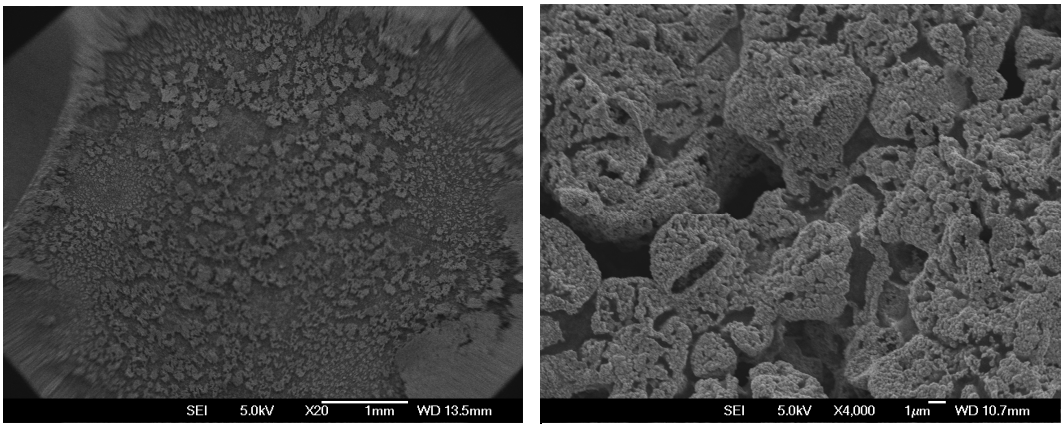

Fig 4.10 FESEM images of top view of PAA-11-4. (Left) An overview of the drop coated area. (Right) A closer look at the middle area.

As shown in Fig 4.7, there was no CNT grown and not even any amorphous carbon deposited on PAA-11-1. It was found that CNTs were grown from the Co-loaded area of PAA-11-2 and PAA-11-3 as shown in Figs 4.8 and 4.9. Fig 4.10 shows that amorphous carbon was deposited on PAA-11-4. These results indicate that Co catalyst is essential for CNT growth. Moreover, an appropriate deposition method is also important since the simple drop-coating method gave amorphous carbon blocks on PAA-11-4, while relatively uniform growth of CNTs was found on PAA-11-2. However, there were only a few CNTs grown on PAA-11-3, despite a longer catalyst deposition time for PAA-11-3 than for PAA-11-2. This may indicate that deposition duration i.e. the amount of the Co catalyst deposited, is another important factor for uniform growth of CNTs.

- *Experiment Set 2*

In set 2, a PAA template was cut into 4 pieces. After electrodeposition, each piece was then cut in half and two sets of CNT growth conditions were used. CNTs were grown in the presence and absence of water vapour. The experimental conditions are shown in Table 4.7.

Table 4.7 Experimental conditions for the preparation of PAA, deposition of Co and growth of CNTs (Set 2)

<table>
<tr><td>Preparation of PAA</td><td colspan="2">PAA-12 (30 V, 0.4 M oxalic acid, 16 ± 1 ºC, 1000 rpm, 2 h/1 h Voltage drop from 30 V to 10 V at a rate of ~ 1 V/ min followed by chemical etching in 0.1 M phosphoric acid at ~30 ºC for 1 h.)

PAA-12 was cut into 4 pieces:
PAA-12-1, PAA-12-2, PAA-12-3 and PAA-12-4</td></tr>
<tr><td>Electrolyte</td><td colspan="2">A solution containing 240 g/L of $CoSO_4$-$7H_2O$ and 40 g/L boric acid (pH ~ 4)
All samples were soaked in the electrolyte overnight on a orbital shaker before electrodeposition</td></tr>
<tr><td>Electrodeposition conditions</td><td colspan="2">10 V_{peak}, 100 Hz square waveform with reductive/oxidative (5 ms/5 ms) pulse polarity

i) PAA-12-1: Electrodeposition under the above conditions for 30 s.
ii) PAA-12-2: Electrodeposition under the above conditions for 3 min.
iii) PAA-12-3: Electrodeposition under the above conditions for 6 min.
iv) PAA-12-4: Electrodeposition under the above conditions for 10 min.

Each sample was then cut in half:
PAA-12-1-1, PAA-12-1-2
PAA-12-2-1, PAA-12-2-2
PAA-12-3-1, PAA-12-3-2
PAA-12-4-1, PAA-12-4-2

All samples were rinsed with DW and then immersed in DW on an orbital shaker overnight before carrying out the CNT growth step.</td></tr>
<tr><td rowspan="2">CNT growth conditions</td><td>PAA-12-1-1,
PAA-12-2-1,
PAA-12-3-1,
PAA-12-4-1,</td><td>The samples were reduced at 500 ºC for 1 h with gas flows of Ar: 1000 sccm and H_2: 800 sccm. Then, CNTs were grown at 600 ºC for 10 min with gas flows of Ar: 1000 sccm, H_2: < 100 sccm and C_2H_4: 400 sccm</td></tr>
<tr><td>PAA-12-1-2
PAA-12-2-2
PAA-12-3-2
PAA-12-4-2</td><td>The samples were reduced at 500 ºC for 1 h with gas flows of Ar: 1000 sccm and H_2: 800 sccm. Then, CNTs were grown at 600 ºC for 10 min with gas flows of Ar: 1000 sccm, H_2: < 100 sccm, C_2H_4: 400 sccm and Ar/H_2O: 25 sccm.</td></tr>
</table>

For all samples in Set 2, a color change and formation of H_2 bubbles were observed as soon as the voltage was applied. After electrodeposition, PAA-12-1 had a brownish color, and the other samples had a bluish color. After CNT growth, a black layer was seen on the Co-loaded area of all samples.

FESEM images of top view of these samples are shown in Figs 4.11-4.18.

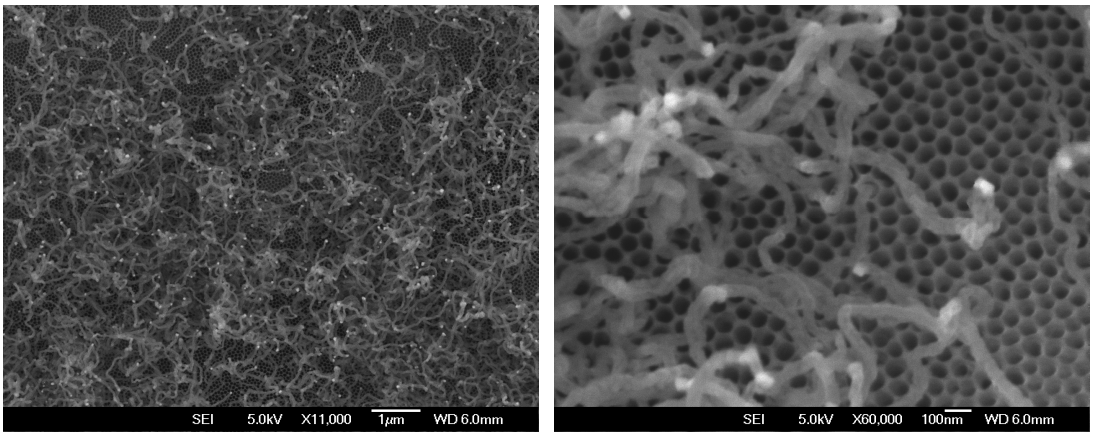

Fig 4.11 FESEM images of top view of PAA-12-1-*1*. (Left) The middle part of CNT growth area. (Right) A closer look at the area.

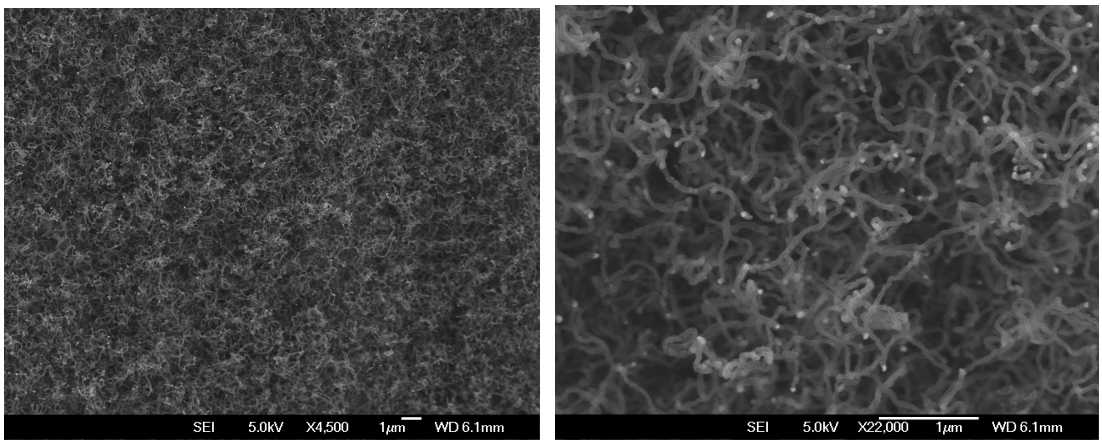

Fig 4.12 FESEM images of top view of PAA-12-1-*2*. (Left) The middle part of CNT growth area. (Right) A closer look at the area.

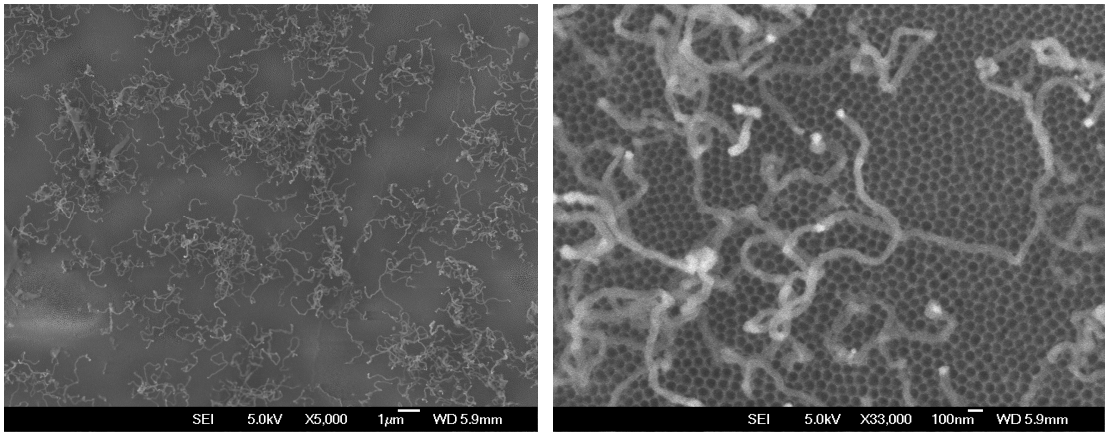

Fig 4.13 FESEM images of top view of PAA-12-2-*1*. (Left) The middle part of CNT growth area. (Right) A closer look at the area.

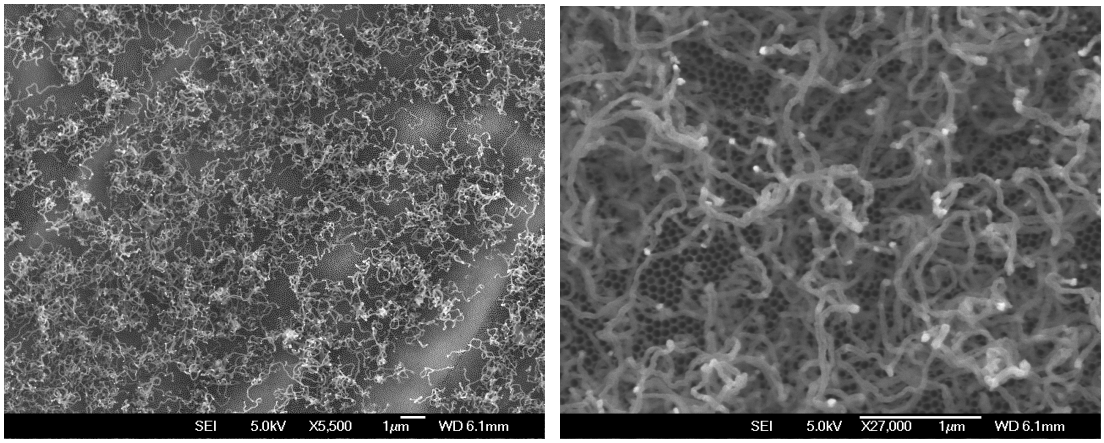

Fig 4.14 FESEM images of top view of PAA-12-2-*2*. (Left) The middle part of CNT growth area. (Right) A closer look at the area.

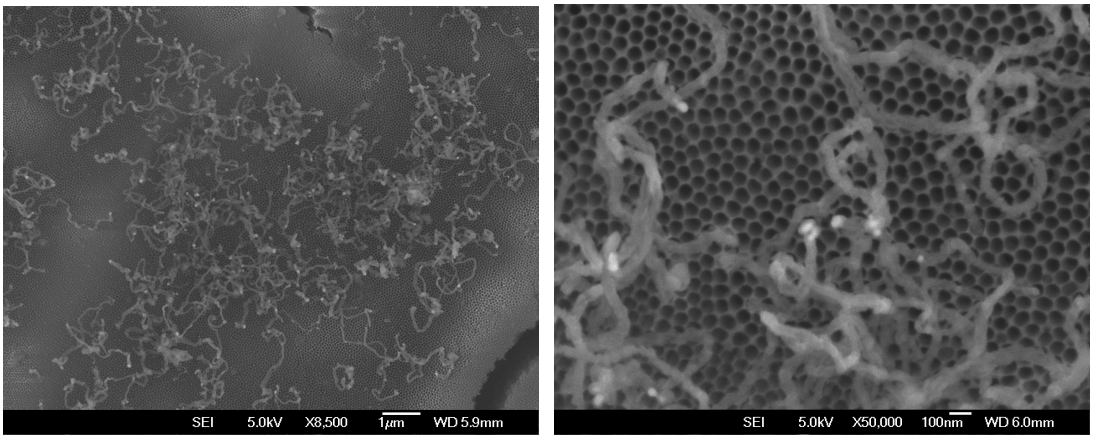

Fig 4.15 FESEM images of top view of PAA-12-3-*1*. (Left) The middle part of CNT growth area. (Right) A closer look at the area.

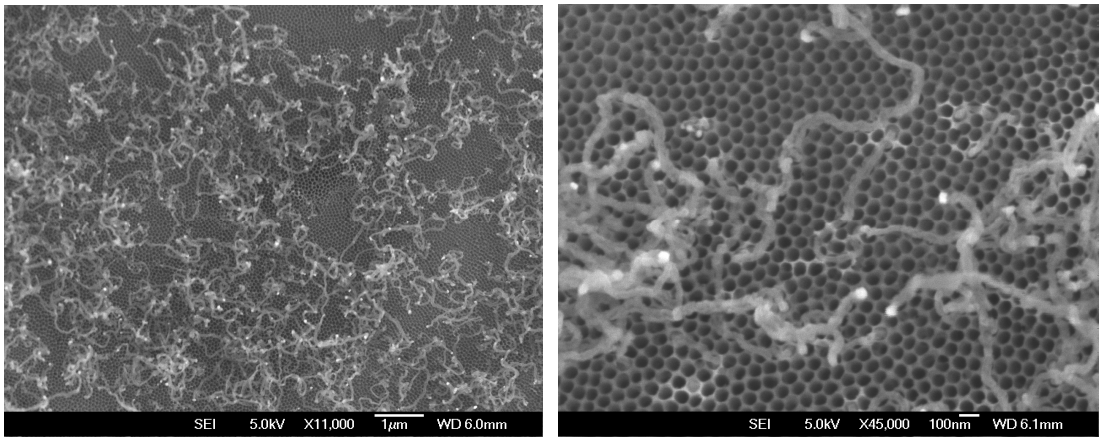

Fig 4.16 FESEM images of top view of PAA-12-3-*2*. (Left) The middle part of CNT growth area. (Right) A closer look at the area.

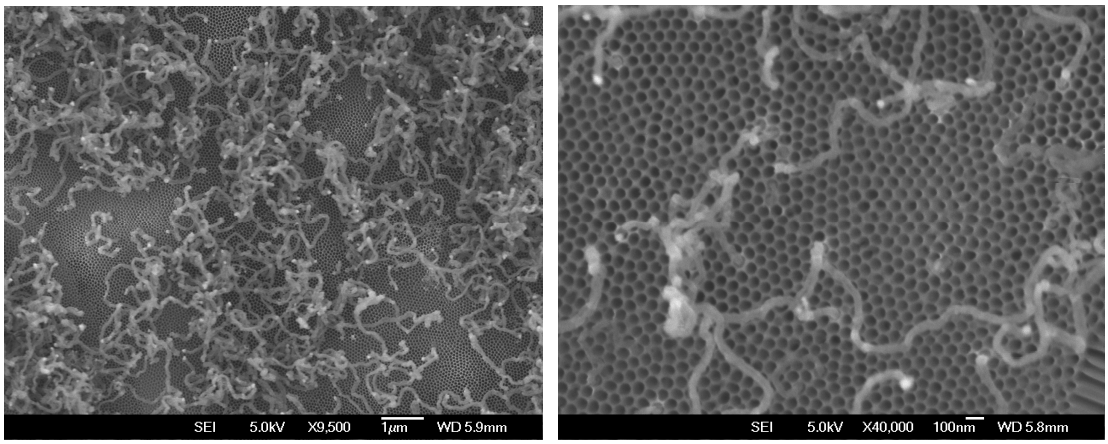

Fig 4.17 FESEM images of top view of PAA-12-4-*1*. (Left) The middle part of CNT growth area. (Right) A closer look at the area.

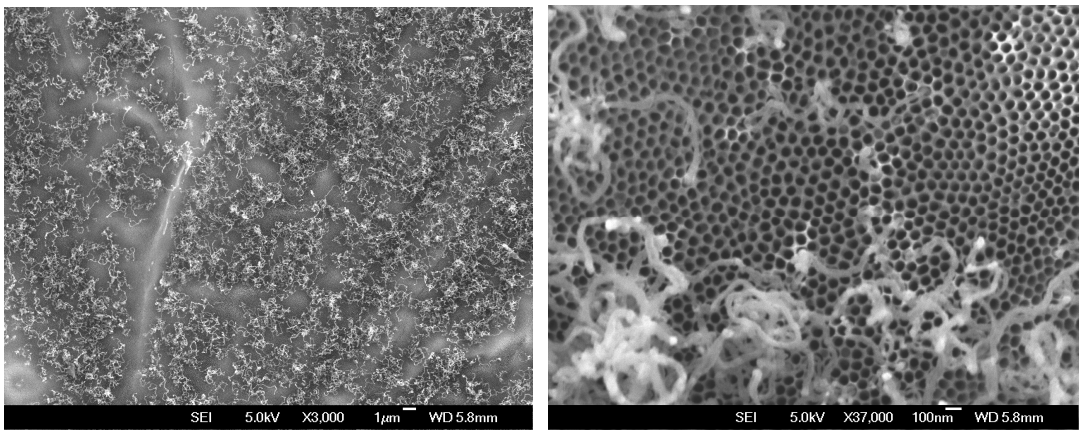

Fig 4.18 FESEM images of top view of PAA-12-4-*2*. (Left) The middle part of CNT growth area. (Right) A closer look at the area.

As shown in Figs 4.11-4.18, CNTs were grown on all samples. However, the quality of the grown CNTs in terms of uniformity, density, tube diameter and length varied due to different conditions as summarised in Table 4.8.

Table 4.8 Effects of experimental conditions on the CNT quality

Sample	**Experimental condition variations**		**CNT growth uniformity**	**Density (surface coverage)**	**CNT diameter (nm)**	**Average length of CNT out of the pore (• m)**
	t- dep [a]	Ar/H_2O [b]				
PAA-12-1-*1*	30 s	No	Uniform	~ 80%	35-50	2
PAA-12-2-*1*	3 min		Not uniform	~30%	~45	2.5
PAA-12-3-*1*	6 min		Not uniform	25-30%	~45	2.5
PAA-12-4-*1*	10 min		Relatively uniform	50-60%	30-45	2
PAA-12-1-*2*	30 s	Yes	Uniform	> 90%	30-50	2
PAA-12-2-*2*	3 min		Relatively uniform	~ 50%	30-45	2
PAA-12-3-*2*	6 min		Relatively uniform	35-45%	30-45	1.5
PAA-12-4-*2*	10 min		Relatively uniform	~ 50%	35-45	2

[a] : Electrodeposition time

[b] : Use of Ar/H_2O flow during CNT synthesis

Higher density CNT growth is observed in the presence of Ar/H_2O flow during CNT growth. This is consistent with the cleaning effect of water vapour, which etches away amorphous carbon from the catalyst and thus facilitates CNT growth. It is observed that the grown carbon nanotubes have a uniform diameter of ~45 nm, which is close to the average pore diameter of ~50 nm. There is a wider range of CNT diameters when the growth is in the presence of Ar/H_2O flow, but this may simply be a consequence of the larger number of CNTs. The average length of the CNT grown out of the pores is difficult to measure since they are not straight and overlap with each other. However, the estimated average lengths in Table 4.7 are consistent with a relatively uniform rate of CNT growth for all samples during the same growth time.

As shown in Figs 4.11-4.18, individual CNTs were grown out of the pores, having a bright dot at its tip. The same observations were found on PAA-11-2, as shown in Fig 4.8. It is assumed that the bright dots are the Co catalyst that was deposited in the pores. This result indicates that the CNT growth mechanism is the tip growth mode under the given conditions, which is consistent with the work that has been done by other research groups[7, 9].

The CNT growth on PAA templates is affected by not only the CNT growth conditions as discussed above, but also the electrodeposition conditions. As shown in Table 4.8, PAA-12-1, for which Co catalyst has been deposited for 30 s, had a more uniform CNT coverage than other PAA-12 samples, and the densest CNT growth. For

Set 1, PAA-11-2 with 30 s deposition time also showed more dense CNT growth than PAA-11-3 with 150 s electrodeposition. These results indicate that electrodeposition time, i.e. the amount of Co deposited, is another important factor for CNT growth. It is assumed that at longer deposition times, the amount of Co deposited prevents favourable interaction of the Co catalyst with the alumina at the pore base. In this case, electrodeposition using the electrolyte containing 240 g/L of $CoSO_4$-$7H_2O$ and 40 g/L boric acid for 30 s gives the best CNT growth.

It is observed that carbon nanotubes were not grown from each pore as shown in previous FESEM images. Since the uniformity of the Co deposited at the bottom of the pores was simply examined by the uniformity of the color by visual observation after the electrodeposition, it is likely that the Co catalyst was not deposited in each pore. Moreover, the origin of the different color on the surface after electrodeposition is unknown. Therefore, it is unlikely to grow carbon nanotubes from each pore in PAA templates.

Unfortunately, the CNTs grown from the PAA templates were not vertically aligned. It is assumed that the overgrowth of CNTs out of the pores affects vertical alignment. The pores act as templates to confine the growth of the CNTs, making them well aligned along the pore walls. However, the part of the CNT grown out of the pores is unsupported, and the vertical alignment is likely to be challenged by the length of the unsupported part of the CNT. Clearly, the vertical alignment is more likely to fail with

an increasing length of the unsupported part of CNTs. It is assumed that the tip growth mechanism of CNTs observed in earlier experiments also affects the vertical alignment. In tip growth mode, the Co catalyst deposited at the bottom of the pores leads the growth of CNTs, after growing out of the template, their growth direction become more random with the increase of the synthesis time, and the Co catalyst is trapped in the CNT tips after CNT growth. Clearly, CNTs with a long unsupported part are less likely to be aligned with a heavy metal head.

However, the base part of the CNTs in the pores is assumed to be vertically aligned by the pore wall. Therefore, VACNTs can be obtained after a cutting treatment[1],[4],[9]. When a cutting treatment such as ultrasonic vibration or ion milling is adopted, the protruded part of CNTs is cut off PAA surface, while the well-aligned part of the CNTs in the pores is preserved. During the treatment, the metal catalyst on the top of the CNTs is also cut away. The PAA membrane then can be dissolved to show the catalyst-free and end-open, well-aligned carbon nanotubes.

4.3 Conclusions

Three barrier layer thinning processes were examined. The results showed that the two-step barrier layer thinning method improved the quality of AC electrodeposition of Co at the bottom of the pores of PAA templates. The electrodeposition conditions

(voltage, waveform, frequency, polarity and electrolyte) were fixed and a suitable range of electrodeposition duration was determined to be 30 s to 10 min.

A set of specified experiments (Set 1) showed that electrodeposition of Co at the bottom of the pores was essential for CNTs growth from PAA templates. Another set of experiments (Set 2) showed that CNT density was affected by the presence of water vapour during CNT growth. Moreover, the CNT growth on PAA templates was also affected by the electrodeposition duration i.e. the amount of Co deposited, and the results showed that 30 s electrodeposition under the given conditions gave the best CNT growth on PAA templates.

Individual CNTs were grown out of the pores with the tip growth mechanism. However, vertical alignment failed on each CNT due to overgrowth of the CNTs and the tip growth mechanism. Although the protruded part of the CNTs was not aligned, the base part of the CNTs inside of the pores is assumed to be vertically aligned by the pores. Therefore, after removal of the random part of the CNTs by a cutting treatment, catalyst-free and end-open, vertically aligned CNTs can be obtained.

References

[1] J. Li, C. Papadopoulos, J. M. Xu and M. Moskovits, *Applied Physics Letters* **1999**, *75*, 367-369.
[2] G. Sharma, M. V. Pishko and C. A. Grimes, *Journal of Materials Science* **2007**, *42*, 4738-4744.
[3] K. Nielsch, F. Muller, A. P. Li and U. Gosele, *Advanced Materials* **2000**, *12*, 582-586.
[4] J. S. Suh and J. S. Lee, *Applied Physics Letters* **1999**, *75*, 2047-2049.
[5] T. Iwasaki, T. Motoi and T. Den, *Applied Physics Letters* **1999**, *75*, 2044-2046.
[6] S. H. Jeong, H. Y. Hwang, K. H. Lee and Y. Jeong, *Applied Physics Letters* **2001**, *78*, 2052-2054.
[7] S. H. Jeong, O. J. Lee, K. H. Lee, S. H. Oh and C. G. Park, *Chemistry of Materials* **2002**, *14*, 4003-4005.
[8] J. S. Lee, G. H. Gu, H. Kim, K. S. Jeong, J. Bae and J. S. Suh, *Chemistry of Materials* **2001**, *13*, 2387-2391.
[9] J. M. Xu, X. B. Zhang, C. Fei, T. Li, Y. Li, X. Y. Tao, Y. W. Wang and X. J. Wu, *Applied Surface Science* **2005**, *239*, 320-326.
[10] L. Kim, E. M. Lee, S. J. Cho and J. S. Suh, *Carbon* **2005**, *43*, 1453-1459.
[11] S. S. Fan, M. G. Chapline, N. R. Franklin, T. W. Tombler, A. M. Cassell and H. J. Dai, *Science* **1999**, *283*, 512-514.
[12] D.-C. Li, L. Dai, S. Huang, A. W. H. Mau and Z. L. Wang, *Chemical Physics Letters* **2000**, *316*, 349-355.
[13] X. Liu, K. H. R. Baronian and A. J. Downard, *Analytical Chemistry* **2008**, *80*, 8835-8839.
[14] N. J. Gerein and J. A. Haber, *Journal of Physical Chemistry B* **2005**, *109*, 17372-17385.
[15] A. Belwalkar, E. Grasing, W. Van Geertruyden, Z. Huang and W. Z. Misiolek, *Journal of Membrane Science* **2008**, *319*, 192-198.
[16] Z. X. Su, G. Hahner and W. Z. Zhou, *Journal of Materials Chemistry* **2008**, *18*, 5787-5795.
[17] K. Nielsch, J. Choi, K. Schwirn, R. B. Wehrspohn and U. Gosele, *Nano Letters* **2002**, *2*, 677-680.
[18] D. Borissov, S. Isik-Uppenkamp and M. Rohwerder, *Journal of Physical Chemistry C* **2009**, *113*, 3133-3138.
[19] J. Li, M. Moskovits and T. L. Haslett, *Chemistry of Materials* **1998**, *10*, 1963-1967.

Chapter 5: Conclusions and Future Work

Synthesis of carbon nanotubes using porous anodic alumina templates via thermal CVD was investigated in this thesis. A two-step anodization process on non-electropolished Al foils was used to produce well-ordered PAA templates. The pore formation during the two-step anodization process was carefully studied. The effects of anodizing conditions on the formation of the PAA membrane were examined. The ordering of the pore arrangement on the membrane surface significantly improved with an increase in the 1st anodization duration, and 1^{st} anodization of 2 h was found to be the optimal condition in terms of ordering of the pore arrangement and time efficiency. The 2^{nd} anodization duration was found to have less influence on the pore arrangement than the 1^{st} anodization, however it determines the final membrane thickness. A linear relationship was observed between the anodizing duration and the membrane thickness, showing a membrane growth rate of 3.7 • m/h under the given conditions. Moreover, the pore diameter was found to vary with the anodizing temperature.

Electrodeposition of Co catalyst at the bottom of the pores by applying an alternating current was investigated under different deposition times. The results established a suitable range of electrodeposition duration. Prior to the electrodeposition, the barrier layer at the bottom of the pores of the PAA template was thinned by a gradual voltage

drop at the end of the 2nd anodization followed by a chemical etching process. This two-step barrier layer thinning process was used because it allowed a superior uniform pore filling by AC electrodeposition.

Carbon nanotubes were successfully grown from the Co-loaded PAA templates using thermal CVD. Characteristics of the grown CNTs in terms of tube diameter, length and density were examined. Individual CNTs with a relatively uniform tube diameter similar to the pore diameter were grown out of the pores with the tip growth mechanism. Length of the CNTs outside of the pores was estimated showing a relatively uniform growth rate. It has been shown that the Co catalyst is essential to the growth of CNTs. Therefore, density of the grown CNTs (or uniformity of the CNT growth) strongly depends on the uniformity of the Co catalyst deposited at the bottom of the pores. Moreover, the CNT density is also affected by the amount of Co deposited at the bottom of the pores and the use of water vapour during the CNT growth. Although vertical alignment of the protruded part of the CNTs failed, the base part of the CNTs inside of the pores was assumed to be vertically aligned.

For future work, a cutting process such as ultrasonic vibration or ion milling could be adopted to remove the random part of the CNTs outside of the membrane. Then the PAA membrane could be partially dissolved in order to obtain the vertically aligned part of the CNTs on the PAA template. Further attempts to grow CNTs under different conditions other than those investigated in this thesis could be undertaken,

and effects of the different conditions on the CNT growth could be studied.

Rigorous examinations on the uniformity of the pore filling by AC electrodeposition could be undertaken in order to gain a better understanding of this process. Different metal catalysts could be deposited at the bottom of the pores and then used for CNT growth. Effects of the use of different metal catalysts on the CNT growth could be examined.

Perfection of the ordering of the PAA membrane could be undertaken. Patterned PAA templates could be prepared by using a pre-pattern-guided anodization approach, and the patterned PAA template then could be used to grow patterned VACNTs.